Full-dimensional diabatic potential energy surfaces including dissociation: The 2E state of NO3

Wolfgang Eisfeld, Olivier Vieuxmaire, Alexandra Viel

Full-dimensional diabatic potential energy surfaces including dissociation: The 2 E state of NO3

Wolfgang Eisfeld, Olivier Vieuxmaire, and Alexandra Viel

Citation: The Journal of Chemical Physics **140**, 224109 (2014); doi: 10.1063/1.4879655
View online: http://dx.doi.org/10.1063/1.4879655
View Table of Contents: http://scitation.aip.org/content/aip/journal/jcp/140/22?ver=pdfcov
Published by the AIP Publishing

Full-dimensional diabatic potential energy surfaces including dissociation: The $^2E''$ state of NO_3

Wolfgang Eisfeld,[1,a)] Olivier Vieuxmaire,[2,b)] and Alexandra Viel[2,c)]
[1]*Theoretische Chemie, Universität Bielefeld, Postfach 100131, D-33501 Bielefeld, Germany*
[2]*Institut de Physique de Rennes, UMR 6251, CNRS and Université de Rennes 1, F-35042 Rennes, France*

(Received 28 February 2014; accepted 6 May 2014; published online 12 June 2014)

A scheme to produce accurate full-dimensional coupled diabatic potential energy surfaces including dissociative regions and suitable for dynamical calculations is proposed. The scheme is successfully applied to model the two-sheeted surface of the $^2E''$ state of the NO_3 radical. An accurate potential energy surface for the NO_3^- anion ground state is developed as well. Both surfaces are based on high-level *ab initio* calculations. The model consists of a diabatic potential matrix, which is expanded to higher order in terms of symmetry polynomials of symmetry coordinates. The choice of coordinates is key for the accuracy of the obtained potential energy surfaces and is discussed in detail. A second central aspect is the generation of reference data to fit the expansion coefficients of the model for which a stochastic approach is proposed. A third ingredient is a new and simple scheme to handle problematic regions of the potential energy surfaces, resulting from the massive undersampling by the reference data unavoidable for high-dimensional problems. The final analytical diabatic surfaces are used to compute the lowest vibrational levels of NO_3^- and the photo-electron detachment spectrum of NO_3^- leading to the neutral radical in the $^2E''$ state by full dimensional multi-surface wave-packet propagation for NO_3 performed using the Multi-Configuration Time Dependent Hartree method. The achieved agreement of the simulations with available experimental data demonstrates the power of the proposed scheme and the high quality of the obtained potential energy surfaces. © *2014 AIP Publishing LLC*. [http://dx.doi.org/10.1063/1.4879655]

I. INTRODUCTION

The dynamics of chemical systems in the presence of strong state-state interactions is a fascinating topic and its fundamental understanding is of high significance. Particularly, the presence of conical intersections and the resulting breakdown of the Born-Oppenheimer approximation has been of great interest.[1] It has been recognized early on that a diabatic or rather *quasi*-diabatic representation of the electronic Hamiltonian and corresponding potential energy matrix is of considerable advantage for the full treatment of the coupled states problem.[2–14] Utilizing the diabatic representation in its simplest form by the linear vibronic coupling model has been an early and extremely successful approach for the explanation of many phenomena in ultra fast nuclear dynamics.[15] Unfortunately, the success of the standard linear vibronic coupling model has been limited to processes that are entirely dominated by the short-time dynamics because in this case only a very small part of the coupled potential energy surfaces (PESs) is of importance and needs to be described qualitatively correctly. Many processes are not of this kind and would require accurate PESs over an extended nuclear configuration space. For this reason it is important to develop methods to generate and represent coupled PESs that are accurate over a larger range of nuclear configurations.

Before we give an overview over various approaches known in the literature, we would like to point out a few aspects of relevance to our development. Good overviews over the topic of the diabatic representation and diabatization can be found in Ref. 1 (especially Chaps. 1 and 4) and Refs. 2, 14, and 15. First of all it is to be understood that there is no direct access to a diabatic representation of the electronic Hamiltonian.[1] All approaches are necessarily based on transformations of adiabatic data, which can be obtained by standard electronic structure calculations.[5,16] A unique and truly diabatic representation cannot be strictly defined in general and it might be better to speak of a *quasi*-diabatic representation.[8,14] In the following we will still use the term "diabatic" rather than "*quasi*-diabatic" simply out of convenience for the reader. The requirement for a suitable diabatic representation is that it minimizes the remaining derivative coupling among the states in the model and the states not included into the model to a degree that it can be neglected like in the standard Born-Oppenheimer approximation.[14] All strong nonadiabatic couplings among the states of interest, particularly the singularities in the coupling operators at conical intersections, are transformed to nondiabatic couplings, which renders the diabatic potential matrix non-diagonal. The advantage of the diabatic representation is that all diabatic energies and couplings must be smoothly varying functions of the nuclear coordinates and one can assume fairly simple functional forms for them.[15] This will be of importance later on. Since nonadiabatic effects and strong state-state couplings usually go hand in hand with complicated electronic structure,

a)wolfgang.eisfeld@uni-bielefeld.de
b)Current address: LPCQ, UMR 5626, CNRS & Université Paul Sabatier, F-31062 Toulouse, France.
c)alexandra.viel@univ-rennes1.fr

we must be aware of the problem of data acquisition.[17] We might face problems with the required *ab initio* calculations in terms of convergence of data points as well as with computational cost. Therefore, we seek for a method that can be based on a minimal number of *ab initio* data points. For the same reason we would like to avoid the time consuming evaluation of nonadiabatic coupling elements, which anyway becomes cumbersome in the vicinity of state intersections. If the number of data points can be reduced, the accuracy of each data point may be increased, which is another reason for this request. In this respect, the symmetry of the system is of major importance because it usually poses tight restrictions on the form of the diabatic potential matrix since the total Hamiltonian must transform as the totally symmetric irreducible representation of the symmetry transformation group.[18] This can and must be utilized in any accurate representation of the electronic Hamiltonian. Finally, one must keep in mind that for a full treatment of the system in question dynamics calculations are to be performed, which have to evaluate the potential energy matrix many times. Thus, a final requirement for a suitable diabatic representation is that it can be evaluated efficiently.

Among the few established methods to treat the coupled states problem, the linear vibronic coupling approach by Köppel, Domcke, and Cederbaum is by far the most widely used and successful.[15] It is certainly the most efficient way to represent the diabatic Hamiltonian of a strongly coupled system because only very few *ab initio* data are required to determine the fairly few coupling and potential parameters. Only adiabatic energies are needed and the adiabatic-diabatic transformation is determined by the diabatic *ansatz*. Unfortunately, the suitability of this approach is limited to processes, which are entirely dominated by the short-time dynamics as mentioned above. In some cases, this problem might be overcome by using the scheme of the regularized diabatization.[19] Other early methods also use an *ansatz* for the diabatic potential matrix elements, though a much more flexible one than just linear or quadratic couplings.[10,20] The smoothness of electronic properties like dipole and transition moments have been utilized to find the appropriate adiabatic-diabatic transformation.[7,21] A lot of scientific effort has been devoted to direct diabatization techniques by which diabatic energies and nondiabatic couplings can be determined from the electronic wave functions within the framework of electronic structure methods.[22–34] Some of these methods rely on a reference point for the diabatization while others compute and annihilate the nonadiabatic coupling elements. For the latter approaches the advent of analytic evaluation techniques of the derivative couplings within the framework of multiconfiguration-reference configuration interaction (MRCI) has been of major importance.[35] The *ab initio* determination of diabatic matrix elements may be used directly in direct dynamics applications if their evaluation is sufficiently fast.[36,37] However, for accurate quantum dynamics treatments this direct evaluation quickly becomes unfeasible and a representation of the diabatic Hamiltonian in closed form is much more suitable. Therefore, one faces the same problems as for the generation of global PESs for a single uncoupled state. The main difference is that a representation of each diabatic matrix element is required. A major breakthrough in the representation of high-dimensional global PESs was achieved by Collins and Parsons[38] by introducing redundant coordinate sets and the full use of the complete nuclear permutation inversion (CNPI) symmetry combined with a modified Shepard interpolation scheme.[39] Such Shepard interpolations were then extended to the representation of diabatic Hamiltonians by Evenhuis and Collins.[40–42] Another modern method to represent high-dimensional global PESs in a more or less generic way was developed by Braams and Bowman[43] and is based on similar principles of redundant coordinates and use of the complete nuclear permutation (CNP) symmetry. The main difference is that symmetry invariant polynomials are used to expand and fit the PES rather than interpolating it. This method has been applied to represent a diabatic Hamiltonian only very recently.[44–46] A very recent modification of the method by Bowman and Braams[43] is the use of neural networks in connection with CNP invariant polynomials but so far this method is limited to single adiabatic PESs.[47,48] Another possibility is the double many-body expansion by Varandas and co-workers.[20,49] Our own approach is closely related to the use of symmetry invariants but originates from vibronic coupling theory. So far we have used point group symmetry (which in our case is isomorphic to CNPI symmetry) and expanded the diabatic Hamiltonian in properly symmetrized coordinates and polynomials for typical Jahn-Teller systems.[50–53] This strategy was also followed by some other groups.[54–57] The present work is an extension of our method to allow for a highly accurate representation of Jahn-Teller systems including the proper direct dissociation asymptotes.

Our system of choice is the nitrate radical (NO_3), which offers a wide range of complications and makes it an ideal test case. There is also considerable interest in this radical due to its importance in atmospheric chemistry,[58] which we will not focus on in the context of the present study. The first problem is the very complicated electronic structure that requires special treatments to avoid artifacts. Even the electronic ground state is not easily computed by standard *ab initio* methods due to a very strong tendency to artificial symmetry-breaking of the electronic wave function.[17] The first two excited states are both doubly degenerate, giving rise to fairly strong Jahn-Teller couplings and the second excited state interacts strongly with the ground state by *pseudo*-Jahn-Teller coupling. A reliable computation of the adiabatic energies of this system requires a fairly elaborate and computationally demanding MRCI treatment of the first five electronic states.[59] A single-reference treatment of the dissociative PESs is inappropriate and will lead to artifacts and qualitatively wrong results.[60] The vibronic coupling problem of the ground state has been treated successfully before[61,62] within the linear vibronic coupling approach but no extended PES has been developed. The treatment of the first excited state was by far less satisfactory[63–66] and thus this state will be our main target of the present study. This first excited state of $^2E''$ symmetry, though predicted before theoretically,[67] was first observed in a photoelectron detachment spectrum in 1991.[68] Much later it was also measured in direct absorption by cavity ring-down spectroscopy.[69,70] Both spectra are fairly resolved

but show complicated perturbations due to the strong nonadiabatic interactions. Thus, such spectra are an excellent test for the accuracy of the coupled surfaces developed in the present work and may allow for a deeper insight into the complicated dynamics involved in the process.

II. THEORY

A. Coordinates

The importance of the choice of coordinates is well known in quantum dynamics. A wise choice of the coordinate system is as important for the accurate analytic representation of PESs. Any suitable coordinate system to represent a global PES needs to allow for the correct description of the complete nuclear transformation symmetry as well as for the right asymptotic behaviour. The set of all inverse pairwise distances between atoms of a molecule, which is overcomplete for systems with more than 4 atoms, fulfills most of these conditions. It is not suitable in general to represent inversion motions properly. This was already recognized by Collins and co-workers, who introduced dot-cross product coordinates to avoid this problem.[42] However, the correct treatment of inversion symmetry by the coordinate set only matters for functions, which transform antisymmetrically with respect to inversion, which explains why inverse pairwise distances can be used for the representation of a single uncoupled PES. For a diabatic representation of a set of electronic states the proper inversion behaviour might be required as in the present case of NO_3. Therefore, a signed coordinate is required and introduced, which describes the inversion motion properly. The definition of the coordinates used for expressing the PES in the present work is displayed in Fig. 1.

The three oxygen atoms are labeled clockwise and the corresponding distances to the central nitrogen atom are labeled r_1, r_2, r_3. The trisector is a line going through the nitrogen atom, which is defined such that the angles between the trisector and each of the N–O bonds are identical. It is indicated as a vertical dashed line in Fig. 1. The corresponding unique angle is the trisector angle ϑ and our special, signed inversion coordinate θ is this trisector angle phase shifted by $\pi/2$ so that $\theta = 0$ corresponds to a planar nuclear configuration. This coordinate could be added to an overcomplete set of coordinates and the remaining motions might be expressed by inverse pairwise distances. However, it turns out that this is a fairly poor choice in the present case and probably in general for bound state problems. If we are willing to assume that the harmonic approximation is not totally wrong for a fairly stiff system like NO_3, we will acknowledge that, according to the harmonic normal coordinates, there are bending and stretching modes, which mix only moderately and are well separated in level energies. However, with a coordinate set of all inverse pairwise distances, the two types of motions cannot be separated in general. This means that complicated coupling terms are required to describe the potential energy along predominant molecular motions in such a set of coordinates. We found during the present work that the coordinate correlations when using only inverse pairwise distances corrupt the accuracy of the PES fits. Therefore, we devise a different strategy by partitioning the coordinate set into stretching, bending, and inversion coordinates to take into account the different characteristics of the various types of nuclear motions. For the bending motions, the angles α_i are used instead of the inverse pairwise O–O distances. These are not the typical valence angles, which would not be independent of the umbrella motion. Instead, the three N–O bonds are projected onto a plane normal to the trisector and the angles between these projected N–O bonds are used to define the α_i. These angles have already been used in Ref. 52. The three projected O–N–O angles are numbered according to the unique atom not involved in forming the angle. For example, the angle formed by the vectors $\boldsymbol{r}_1$ and $\boldsymbol{r}_2$ is symbolized by α_3 and so on.

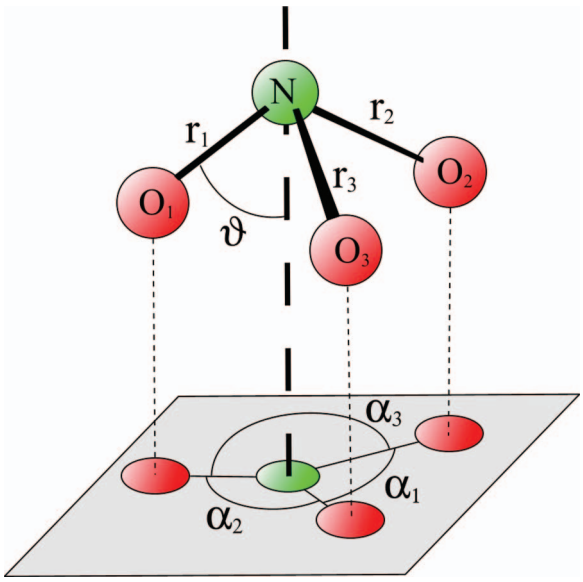

FIG. 1. Definition of the primitive coordinates of NO_3 in terms of distances r_i, projected valence angles α_i, and the trisector angle ϑ.

The coordinates defined above form the primitive coordinate set based on valence coordinates, which is further modified to fulfill the symmetry requirements and to allow for the dissociation of the molecule. The three N–O distances r_i are transformed to what we call tunable Morse type coordinates (TMCs), $m(r_i)$, by

$$m(r_i) = 1 - e^{-f(r_i)(r_i - r_0)} \tag{1}$$

with the exponent function

$$f(r_i) = \alpha + \frac{\beta}{2}(\tanh(\gamma(r_i - r_{ref})) + 1) + e^{-\delta(r_i - r'_{ref})^2} \sum_{k=0}^{n} p_k (r_i - r''_{ref})^k. \tag{2}$$

The distance dependent exponent function is key to obtain ultimate accuracy for the PESs because it tunes the standard Morse coordinate. The detailed analysis of diatomic potential functions showed that expansions in Morse coordinates with constant exponent prefactor are insufficient. A thorough investigation of the distance dependent optimal exponent prefactor led us to the development of the function defined in Eq. (2). The transformation of distances to TMCs ensures that any polynomial expansion in a single such kind of coordinate

will show the correct asymptotic behaviour for a bond dissociation. This is not necessarily so for a multi-dimensional expansion as will be discussed below. The form of this coordinate also covers much of the anharmonicity for typical stretching modes and allows for higher accuracy of the fits with shorter polynomial expansions. The three projected O–N–O angles α_i are transformed to scaled angles α_i' by

$$\alpha_i' = \frac{\alpha_i}{r_j r_k}, \quad i \neq j \neq k, \tag{3}$$

in which the N–O distances r_j and r_k refer to the bonds forming the corresponding angle α_i. This type of scaling describes properly the situation that at any dissociation asymptote some bending motions described by the primitive angles α_i will turn into free rotations and thus the potential needs to become independent of such a coordinate. For the same reason the trisector angle is scaled by a product of all three N–O distances,

$$\theta' = \frac{\theta}{r_1 r_2 r_3}. \tag{4}$$

Finally an auxiliary hyperradius ξ is defined as

$$\xi = r_1 + r_2 + r_3. \tag{5}$$

The transformed distances, scaled angles, scaled trisector angle, and the hyperradius form our overcomplete transformed primitive coordinate set. This set is then symmetrized according to the molecular transformation symmetry group, which is D_{3h} in the present case. The trisector angle transforms like a_2'' and thus already is a symmetry coordinate and the hyperradius is obviously totally symmetric. The subsets of three distances or angles, respectively, form a reducible representation, which decomposes into a_1' and e' irreducible representations. The corresponding Clebsch-Gordan transformation matrix reads

$$\boldsymbol{U} = \begin{pmatrix} \frac{1}{\sqrt{3}} & \frac{1}{\sqrt{3}} & \frac{1}{\sqrt{3}} \\ \frac{2}{\sqrt{6}} & \frac{-1}{\sqrt{6}} & \frac{-1}{\sqrt{6}} \\ 0 & \frac{1}{\sqrt{2}} & \frac{-1}{\sqrt{2}} \end{pmatrix} \tag{6}$$

which transforms the vectors of our equivalent primitive coordinates to a new vector containing the symmetry coordinates transforming as a_1' and e', respectively. However, the symmetric linear combination of the angles is obviously an inappropriate coordinate and is omitted from the set of symmetry coordinates. Thus, we end up with the following six linearly independent and properly symmetrized internal coordinates required to represent the PES of the system:

$$s_1 = \frac{1}{\sqrt{3}}(m(r_1) + m(r_2) + m(r_3)), \tag{7a}$$

$$s_2 = \theta', \tag{7b}$$

$$s_3 = \mathfrak{s}_{3x} = \frac{1}{\sqrt{6}}(2m(r_1) - m(r_2) - m(r_3)), \tag{7c}$$

$$s_4 = \mathfrak{s}_{3y} = \frac{1}{\sqrt{2}}(m(r_2) - m(r_3)), \tag{7d}$$

$$s_5 = \mathfrak{s}_{4x} = \frac{1}{\sqrt{6}}(2\alpha_1' - \alpha_2' - \alpha_3'), \tag{7e}$$

$$s_6 = \mathfrak{s}_{4y} = \frac{1}{\sqrt{2}}(\alpha_2' - \alpha_3'). \tag{7f}$$

This set is complemented by the auxiliary coordinate ξ.

B. Diabatic potential model

In the present study we develop the diabatic Hamiltonian for the separated $^2E''$ first excited state of NO_3 only. Possible couplings to the $^2A_2'$ ground and the $^2E'$ second excited state are not treated yet and will be added in future work. This coupling is entirely due to the inversion motion along the a_2'' mode, which is hardly excited in the experiments because all equilibrium structures remain planar.

The nonadiabatic coupling within the degenerate $^2E''$ state is well understood and depends on the modes of e' symmetry. The requirement that the Hamiltonian needs to transform as totally symmetric poses strict limitations on the form of the matrix elements $h^d_{\alpha\beta}$ of the diabatic Hamiltonian $\boldsymbol{H}^d$, which in general can be expanded as polynomials in terms of the symmetry coordinates as

$$h^d_{\alpha\beta}(\boldsymbol{s}) = \sum_{k=1} c_k^{(\alpha\beta)} \prod_{l=1}^{6} s_l^{n_l}, \quad N = \sum_{l=1}^{6} n_l \leq n_{max}. \tag{8}$$

The upper limit of k depends on the maximum order of the expansion terms, n_{max}. The symmetry restrictions enforce that many of the expansion coefficients are strictly related to each other for every given polynomial order N. These relations can be easily derived using symmetry and invariant theory.[50,51,56,57] For a Jahn-Teller system with a threefold axis as main symmetry element we already derived the proper symmetry polynomials.[50] However, we did not fully treat the possibility of all possible multi-mode couplings before, combining, e.g., the two e' modes. All these symmetry polynomials up to four-body terms (six-body if we consider the components of the e' modes as separate modes) have been derived and implemented for the present study. The critical terms are only the ones depending on the degenerate e' modes, whose symmetry transformation properties according to the $\widehat{C}_3$ rotation can be easily analysed after transformation into the complex plane. One can simply use the results of Table I of Ref. 50 and substitute all the terms by the unique mixed polynomials of the right power in the complex coordinates. Back transformation of the resulting matrices into the real plane yields the properly symmetrized mixed polynomials and their relations in the real Jahn-Teller coupling matrix. All newly derived symmetry polynomials and the explicit form of the diabatic matrix elements are given in the Appendix.

The general structure of the diabatic potential matrix reads

$$\boldsymbol{H}^d(\boldsymbol{s}) = \sum_k a_k \begin{pmatrix} v_k(\boldsymbol{s}) & 0 \\ 0 & v_k(\boldsymbol{s}) \end{pmatrix} + \sum_l b_l \left[\begin{pmatrix} w_l(\boldsymbol{s}) & 0 \\ 0 & -w_l(\boldsymbol{s}) \end{pmatrix} + \begin{pmatrix} 0 & z_l(\boldsymbol{s}) \\ z_l(\boldsymbol{s}) & 0 \end{pmatrix} \right] \tag{9}$$

in which the terms v_k define a diagonal potential $\mathcal{V}$ and the terms w_l and z_l yield the diagonal and off-diagonal Jahn-Teller couplings, $\mathcal{W}$ and $\mathcal{Z}$, respectively. Each matrix element can be broken down according to the coordinates involved and the order of the polynomials. For example, the diagonal potential can be written as

$$\begin{aligned}\mathcal{V}(\boldsymbol{s}) = &\mathcal{V}_a(s_1) + \mathcal{V}_b(s_2) + \mathcal{V}_{e_1}(\mathfrak{s}_{3x}, \mathfrak{s}_{3y}) + \mathcal{V}_{e_2}(\mathfrak{s}_{4x}, \mathfrak{s}_{4y})\\ &+ \mathcal{V}_{ab}(s_1, s_2) + \mathcal{V}_{ae_1}(s_1, \mathfrak{s}_{3x}, \mathfrak{s}_{3y}) + \mathcal{V}_{ae_2}(s_1, \mathfrak{s}_{4x}, \mathfrak{s}_{4y})\\ &+ \mathcal{V}_{be_1}(s_2, \mathfrak{s}_{3x}, \mathfrak{s}_{3y}) + \mathcal{V}_{be_2}(s_2, \mathfrak{s}_{4x}, \mathfrak{s}_{4y})\\ &+ \mathcal{V}_{ee}(\mathfrak{s}_{3x}, \mathfrak{s}_{3y}, \mathfrak{s}_{4x}, \mathfrak{s}_{4y})\\ &+ \mathcal{V}_{abe_1}(s_1, s_2, \mathfrak{s}_{3x}, \mathfrak{s}_{3y}) + \mathcal{V}_{abe_2}(s_1, s_2, \mathfrak{s}_{4x}, \mathfrak{s}_{4y})\\ &+ \mathcal{V}_{aee}(s_1, \mathfrak{s}_{3x}, \mathfrak{s}_{3y}, \mathfrak{s}_{4x}, \mathfrak{s}_{4y})\\ &+ \mathcal{V}_{bee}(s_2, \mathfrak{s}_{3x}, \mathfrak{s}_{3y}, \mathfrak{s}_{4x}, \mathfrak{s}_{4y})\\ &+ \mathcal{V}_{abee}(s_1, s_2, \mathfrak{s}_{3x}, \mathfrak{s}_{3y}, \mathfrak{s}_{4x}, \mathfrak{s}_{4y}) \qquad (10)\end{aligned}$$

and each of the functions is expressed as properly symmetrized polynomial in the required symmetry coordinates. For example, the $\mathcal{V}_{ee}(\mathfrak{s}_{3x}, \mathfrak{s}_{3y}, \mathfrak{s}_{4x}, \mathfrak{s}_{4y})$ up to 6th order contains 28 independent terms consisting of one 2nd order, two 3rd order, four 4th order, eight 5th order, and thirteen 6th order polynomials. As an example we may look at a prototypical 6th order polynomial that reads

$$\begin{aligned}v_{ee}^{(6,1)} = &\mathfrak{s}_{3y}\mathfrak{s}_{4y}^5 - 5\mathfrak{s}_{3x}\mathfrak{s}_{4x}\mathfrak{s}_{4y}^4 - 10\mathfrak{s}_{4x}^2\mathfrak{s}_{3y}\mathfrak{s}_{4y}^3 + 10\mathfrak{s}_{3x}\mathfrak{s}_{4x}^3\mathfrak{s}_{4y}^2\\ &+ 5\mathfrak{s}_{4x}^4\mathfrak{s}_{3y}\mathfrak{s}_{4y} - \mathfrak{s}_{3x}\mathfrak{s}_{4x}^5, \qquad (11)\end{aligned}$$

which shows a distinct linear combination of mixed 6th order terms. Changing the ratio between the coefficients of these linear combinations inevitably will destroy the correct symmetry transformation properties of the PESs. Full details of the derived potential terms are given in the Appendix. The multi-mode terms involving s_1 and s_2 can be written down easily because these coordinates are invariant under the $\widehat{C}_3$ operation. Thus, a term like $\mathcal{V}_{abee}(\boldsymbol{s})$ can be obtained from combining the terms of $\mathcal{V}_{ee}$ with all powers in s_1 and all even powers in s_2. In this case, one only needs to take care of the proper asymptotic behaviour of the multi-mode term because the inversion coordinate turns into a free rotation upon dissociation of any of the three equivalent N–O bonds. This is achieved by transforming the primitive coordinates prior to their symmetrization as explained above. In addition, all terms depending on the umbrella coordinate, s_2, are damped by $e^{-\rho_u \xi}$ using the auxiliary hyperradius ξ, e.g.,

$$\mathcal{V}_{abee}(\boldsymbol{s}) = \sum_n \mathcal{V}_{aee}\left(s_1, s_3, s_4, s_5, s_6; \boldsymbol{p}_{v,abee}^n\right) s_2^n \; e^{-\rho_u \xi}, \quad (12)$$

where ρ_u is a damping parameter and $\boldsymbol{p}_{v,abee}^n$ refers to the parameter vector corresponding to the potential term. Using the $\mathcal{V}(\boldsymbol{s})$ terms alone is sufficient to represent a single uncoupled state such as the anion ground state, which is the initial state for the photoelectron detachment experiment. Therefore, we use exactly this form for the anion ground state PES and expand $\mathcal{V}(\boldsymbol{s})$ up to full 6th order in all terms except the two $\mathcal{V}_{be_i}$ terms, which are expanded up to 8th order. This yields a total of 118 terms of which 92 terms depend only on planar motions and 26 terms also depend on the umbrella coordinate. For the representation of the $^2E''$ state we use exactly the same form for $\mathcal{V}(\boldsymbol{s})$ as for the initial state but additionally expand the Jahn-Teller coupling terms to full 6th order. This adds two times 149 terms to the diabatic Hamiltonian, depending on planar motions only, plus another two times 43 terms involving the umbrella coordinate. Due to the symmetry of the system, the corresponding w_l and z_l terms occur in pairs with a common expansion parameter, so that only 192 additional fitting parameters need to be treated. The resulting set of 310 parameters is complemented by one parameter for the reference energy and one for the radial umbrella damping factor ρ_u. Additional 6 parameters are used for the TMC transformation (Eq. (2)) in which $r_{ref} = r'_{ref} = r''_{ref} = \beta = 0$ are chosen and the polynomial is expanded up to third order.

One major problem in the construction of high-dimensional PESs is the possible existence of regions, where the model yields artificially low energies, which are usually referred to as "holes." If such holes are reachable by a wave-packet or trajectory, the corresponding PES is essentially unusable. The typical reason for the occurrence of holes is the undersampling of the PESs because only a limited number of fitting data can be generated for high-dimensional problems. The regions of interest are usually at low energy and probably including asymptotes and therefore the data sampling is usually concentrated there. As a consequence, the holes are often found in the highly repulsive high energy regions because no fitting data is available there to be accounted for in the fitting process. The problems in the asymptotic regions can be handled quite well by the choice of appropriate coordinates such as the tunable Morse type coordinates, see Eqs. (1) and (2), or inverse distances. The problems in the repulsive walls are not likely to be fixed easily by coordinate transformation. The present approach to deal with this issue is twofold. First, the problematic regions are detected either by statistical sampling or imaginary time propagation of a wave-packet for a given PESs model (see below). Then *ab initio* calculations are performed for points in the detected regions and the results are added to the fitting basis. This may or may not solve the problem for a certain region, depending on the energies of the added fitting points and the corresponding weights in the fit (see below). The second strategy is based on a slightly different representation of the diabatic potential model itself. Instead of using just one polynomial expansion as in Eq. (9), the Hamiltonian is split into two expansions

$$\boldsymbol{H}^d(\boldsymbol{s}) = \boldsymbol{H}_{ref}^d(\boldsymbol{s}) + \sigma(\varepsilon) \cdot \boldsymbol{H}_{corr}^d(\boldsymbol{s}), \qquad (13)$$

in which $\boldsymbol{H}_{ref}^d$ is a low-order expansion called reference model, $\boldsymbol{H}_{corr}^d$ is a correction model that contains all the terms of the full model, Eq. (9), that are not contained in $\boldsymbol{H}_{ref}^d$, and σ is a switching function. The switching functions used are either

$$\sigma(\varepsilon) = \frac{1}{2}\left(1 - \tanh \rho_\varepsilon(\varepsilon - \varepsilon_0)\right) \qquad (14)$$

or

$$\sigma(\varepsilon) = \begin{cases} 1 & x(\varepsilon) < 0 \\ 1 - x(\varepsilon)^2\left(2 - x(\varepsilon)^2\right) & 0 \le x(\varepsilon) \le 1 \\ 0 & x(\varepsilon) > 1 \end{cases}, \qquad x(\varepsilon) = \frac{\varepsilon - \varepsilon_0}{\rho_\varepsilon}, \tag{15}$$

in which ε_0 is a reference energy and ρ_ε is a width parameter, determining the range over which the switching takes place. For the switching parameter ε, either the lowest eigenvalue of the reference model is used or the difference between the lowest eigenvalues of the reference model and the full model, Eq. (9), is utilized. The reference model is defined such that it represents the PESs only roughly but qualitatively correctly. Particularly, in the otherwise problematic regions it must produce sufficiently high energies. Since the holes are always found in regions irrelevant for the physics of the process to be described, it is appropriate to switch to the reference model entirely wherever the energies of the full model fall too far below the values from the reference model. Thus, the PESs are described by the full model with high accuracy in the relevant regions but are only roughly modeled in irrelevant areas where the full model causes problems.

C. Electronic structure methodology and data acquisition

The electronic structure treatment of the anion is mostly uncritical because it is a well-behaved closed-shell molecule and the PES is only required in a limited region around the equilibrium position. Thus, we performed closed-shell coupled-cluster singles doubles with perturbative triples (CCSD(T)) calculations[71] using a fairly large atomic orbital (AO) basis. The correlation consistent aug-cc-pVQZ standard basis was chosen for all atoms.[72,73] To account for the diffuse character of the anion wavefunction, we added a set of [8s,6p,4d,2f] uncontracted basis functions from the set of universal Rydberg functions of Kaufmann *et al.*[74]

By contrast, the *ab initio* treatment of the NO_3 radical is extremely involved. This is partly due to its extreme tendency to artificial symmetry breaking of the electronic wave function.[17] The problem is aggravated further by the necessity to describe excited states and bond ruptures reliably, which requires a multireference treatment. Thus, complete active space self-consistent field (CASSCF)[75,76] is used to generate the reference wave function for a successive multi-configuration reference configuration interaction singles and doubles (MR-SDCI) calculation. The internally contracted MR-SDCI method is used[77,78] and all calculations are performed with the MOLPRO package of *ab initio* codes.[79] The energy data used to fit the PESs are the Davidson corrected MR-SDCI energies.[80] The active space for CASSCF and MR-SDCI calculations contains 17 electrons in 13 active orbitals, which at the D_{3h} ground state equilibrium geometry refer to $[4a_1'\ 3e'\ 4e'\ 1a_2'\ 5a_1'\ 5e'\ 1a_2''\ 1e''\ 2a_2'']$. This large active space results in a huge number of determinants and mainly is needed to avoid artifacts in the reference wave function. Therefore, a common subset of reference configurations was selected for all states according to the coefficients in the CI vectors of the CASSCF reference states. This reference space was completed by adding all missing configurations required to render the configuration space invariant under the D_{3h} symmetry operations. The CI matrix was built by excitations out of reference configurations of all irreducible representations of the respective point group, which is necessary to avoid symmetry breaking at the D_{3h} geometry and makes the energies of all MRCI calculations comparable. Only excitations out of active space orbitals were allowed, excluding the four 1s core orbitals and a low-lying set of a_1' and e' orbitals composed of the 2s AOs from the correlation treatment. Despite the tremendous savings in computational demand due to the selected reference configuration space, we are still limited in the choice of the AO basis. After extensive testing, we chose to use the correlation consistent aug-cc-pVTZ standard basis[72,73] for all atoms but remove the set of diffuse f-functions.[59] This approach yields results for excitation and dissociation energies in excellent agreement with experiment.[59] It also proves to be rather robust, which is extremely important for the development of accurate PESs. Nevertheless, special care needs to be taken in the data generation to avoid spurious results in the data set.

An important question is how to select the nuclear configurations at which to compute the electronic energies. A simple grid approach like for triatomic systems is unfeasible here and due to the computational cost of the *ab initio* calculations, we aim to obtain the most accurate PESs with the least data possible. It is unlikely that any systematic way to generate the nuclear configurations will yield an optimal selection because a six-dimensional system is much to complex to avoid the risk of an unwanted bias. Collins and Ischtwan introduced techniques to use trajectory calculations in order to find the most relevant parts of a PES for a reactive system.[39] However, such an approach does not appear very useful in the present case because classical dynamics is not very suitable for the necessary multi-state treatment required in the present case. Therefore, we devise a statistical approach, which is designed such that a control over the convergence of the MRCI calculations remains possible and the *ab initio* calculations stay robust. Rather than generating random geometries in six dimensions, we use 6D random displacement vectors. These random vectors define cuts through the PESs along which data points are acquired, usually starting in the vicinity of the equilibrium geometry. This allows for the use of a well defined and correctly converged initial guess wave function in order to avoid the problem of spurious convergence of the *ab initio* calculations. This also allows for a quick and simple visual control of the obtained data. Furthermore, the density of points is higher at the bottom of the potential well, where a higher accuracy is needed in our case, and gets sparser in the outer high-energy regions, in which we are not particularly interested. It is possible to include various reference geometries as origins of the random scans so that all important regions of the PESs can be sampled with an appropriate density of points. It is also easy to include or exclude certain asymptotic channels by selecting the allowed coordinate ranges for the elements of the random vectors. In the present study, we are not interested in the high-energy decomposition corresponding to the cleavage of more

than one N–O bond. Therefore, only one N–O distance is allowed to reach the asymptotic region at a time.

D. Fitting methodology

Once the PES model is set up and the *ab initio* points have been acquired, what remains is to determine the optimal parameters. The data for a single PES like that of NO_3^- may be fitted by a standard linear least squares approach, if the nonlinear coordinate transformation is not to be optimized. However, it can be beneficial to use nonlinear optimization techniques even for a single PES although this is much more involved. The fitting of the coupled diabatic PESs unavoidably requires a nonlinear approach due to the diagonalization to obtain the eigenvalues, which have to be fitted with respect to the adiabatic *ab initio* energies.

The approach used in the present study is a dual-layer method of a genetic algorithm[81] into which a usual Marquardt-Levenberg[82] nonlinear least-squares fit is embedded. At the beginning of the optimization, a large number of test parameter sets is created stochastically, starting from user specified initial guess parameters and parameter ranges. A Marquardt-Levenberg fit is carried out for each of these sets from the initial generation. A limited number of the resulting parameter sets with the lowest fitting errors are selected and form the initial parent generation of sets. The next generation of test sets is obtained from scrambling the parameters of the selected parent sets and some arbitrary mutations of randomly selected parameters. Then the next series of Marquardt-Levenberg fits is carried out and from the resulting parameter sets combined with the parent sets the most successful sets are selected as the next generation of parent sets. This procedure is repeated as long as the lowest fitting error decreases.

Another important aspect of the fitting is the weighting of input data. One is mostly interested in the lower energy regions of the PESs while high energy regions are of no interest because the probability that a trajectory or wave-packet will sample such areas is negligible. Therefore, much larger absolute fitting errors are acceptable for very high energies than for low energies. On the other hand, even in very high energy regions data points may be required in order to circumvent problems with holes in the PESs. The way to avoid to compromise the quality of the fit for the important low energy regions is to introduce an energy dependent weighting of the data points. In the present study, a simple exponential decay function

$$\omega_i(E_i) = e^{-\rho_i(E_i - E_{i0})} \tag{16}$$

is used to determine state and energy dependent weights, in which E_{i0} is a reference energy for state i and ρ_i a damping parameter for state i. Additionally, user specified weights are scaled by these computed energy dependent weights and finally the sum of weights is properly normalized.

E. Quantum dynamics

In order to better assess their quality, both the NO_3^- and the two-sheeted coupled NO_3 PESs have been used for dynamical studies in full dimension. Given the six internal degrees of freedom and two electronic surfaces, the MCTDH approach,[83,84] suitable for the representation of wave functions with large dimensionality, is used.

The Hamiltonian operator of the Schrödinger equation for the dynamical studies contains, in addition to the diabatic potential term, the kinetic energy operator. The expression of this kinetic energy operator for numerical evaluation depends on the basis set used in the wave-packet representation as well as on the coordinates. The coordinates used for the potential energy surfaces would lead to a complicated kinetic energy operator that would not be suitable for an efficient MCTDH computation. Therefore, we use the six internal stereographic coordinates introduced in Ref. 85 which leads to an optimal expression for the exact kinetic energy operator. The north pole projection version of the three radial $r_1^{(st)}, r_2^{(st)}, r_3^{(st)}$, the angular $\theta^{(st)}$, and the two orientational $s_3^{(st)}, t_3^{(st)}$ stereographic coordinates as detailed in Ref. 86 are employed. In this coordinate set, planarity corresponds to $t_3^{(st)} = 0$. The corresponding kinetic energy term for a non-rotating NO_3^- or NO_3 given in Ref. 86 respects the sum of products of single particle constraint of MCTDH friendly operators. The potential term does not respect this constraint. For the anion, the evaluation of the potential term is carried out using the CDVR scheme.[87] The generalized version of CDVR as detailed in the Appendix of Ref. 52 is employed for the evaluation of the diabatic two by two potential matrix of the radical.

Two types of calculations have been performed. First, the low vibrational energy levels of the anion are determined using the state average and block diagonalisation scheme.[88] Second, the photodetachment experiment[68] is simulated by assuming a vertical transition of the NO_3^- vibrational ground state eigenfunction onto the two-sheeted surface of the neutral system. The photodetachment spectrum is obtained from the autocorrelation function of this initially prepared wavepacket propagated for 200 fs. The non-adiabatic dynamics is revealed by the adiabatic population computation using the CDVR scheme to evaluate the effect of the projection operator on the propagated wave-packet.[52] For the representation of the wave-packets, Fourier transform grids as given in Table I are used. In this table, we give both the numbers of single particle functions used to determine the lowest eigenstates of the anion and the ones required to study the non-adiabatic dynamics of the NO_3 radical. The range of variation for the six

TABLE I. Wave function representations given by the number of single particle functions (n), the number of Fourier points (N) and the range of the underlying box (in a.u.) for the six stereographic coordinates.

	n			
Coordinate	NO_3^-	NO_3	N	Box range
$r_1^{(st)}$	7	14	64	[352 : 522]
$r_2^{(st)}$	7	14	64	[352 : 522]
$r_3^{(st)}$	7	14	64	[352 : 522]
$\theta^{(st)}$	9	14	32	[1.80 : 2.40]
$s_3^{(st)}$	9	14	32	[− 0.76 : −0.36]
$t_3^{(st)}$	6	4	32	[− 0.17 : 0.17]

coordinates is adapted to the evolution of the wave-packet of the NO_3 radical computation. Note that for the lowest vibrational levels of the anion smaller intervals would be sufficient.

III. RESULTS AND DISCUSSION

A. PES and dynamics of the NO_3^- anion

1. Potential energy surface

The ground state of the nitrate anion (NO_3^-) is a non-degenerate state of $^1A_1'$ symmetry with a D_{3h} equilibrium geometry. Therefore, the PES can be expressed as an uncoupled surface using the $\mathcal{V}$ elements only. The equilibrium distance of the three equivalent bond distances is slightly longer than that of the ground state of the neutral nitrate radical. This is easily understood by the extra electron being located in the slightly anti-bonding a_2' orbital to result in the closed-shell electron configuration of the anion. On the other hand, removing an electron from either of the highest-lying three sets of occupied orbitals of the anion, having symmetries of a_2', e'', and e', results in the three lowest electronic states of the nitrate radical, which are the subject of intense scientific interest. A ground-breaking experiment has been the recording of the photodetachment spectrum of NO_3^-, yielding the first experimental data of the first excited state of $^2E''$ symmetry.[68] This very complex spectrum is not really understood yet and in order to investigate it theoretically, a high-quality PES for the initial state, namely that of NO_3^-, is required.

The PES for the anion only needs to be accurate in the potential well since the initial state is the vibrational ground state and higher vibrational states or reactive processes play hardly any or no role at all, respectively. Therefore, the data acquisition was concentrated in a fairly limited region around the minimum and the dissociation channels were not included. 1700 data points were calculated using the stochastic approach of calculating random cuts through the PES starting from the equilibrium position of the neutral NO_3 ground state. These data were fitted by our model Hamiltonian, resulting in a root mean square (rms) error of 3 cm^{-1}. This excellent result shows both the convergence quality of the underlying *ab initio* data as well as the capability of the model potential used. However, that PES was only good within the limited region of the potential well and caused artificially low energies far outside the well. For a typical bound-state calculation this would not really matter but in the present case the obtained bound state is the initial state for an electron detachment calculation. For technical reasons, it is very convenient to represent the nuclear wave function on the same grid for the NO_3^- and the NO_3 for this calculation. When propagating on the radical states, the nuclear configuration space sampled is much larger than the one necessary for the determination of low vibrational states of NO_3^-. Therefore, the outer regions of the NO_3^- PES had to be improved.

In order to do so, the data basis for the fit was enlarged by 170 data points generated by random cuts, allowing for larger displacements of the bond distances, and 27 data points referring to geometries for which artificially low energies were found by a stochastic sampling scheme testing the model PES. In addition, the split reference and correction model scheme, Eq. (13), was applied with the polynomial switching function, Eq. (15), using the difference of the reference energy and the undamped full model as argument ε. Finally, a restriction on the lowest order parameter for $\mathcal{V}_{ea_1}$ in the reference model was implied, namely that it must not be less than the negative absolute of the lowest order parameter of $\mathcal{V}_{e_1}$. A new fit resulted in a rms error of 17 cm^{-1}, which is still an excellent result. Furthermore, no regions of artificially low energies were found on the new PES, neither by stochastic sampling nor by extensive wave-packet propagations. This final anion PES was used in all of the quantum dynamics calculations reported below.

2. Vibrational states

The lower part of the created surface is tested by computing the seven lowest eigenstates of the anion. The state average and block diagonalisation scheme[88] is used with seven wave-packets in order to obtain the ground state and the first six excited states. Similar to a Lanczos algorithm, the scheme relies on successive imaginary time propagations, $e^{-\beta\hat{H}}$, and diagonalisation steps to create an optimal set of wave-packets to compute the lowest vibrational levels. For the calculations, we use an imaginary time propagation β of 400 a.u. With this value of β, the total number of iterations required to reach an internal precision of 10^{-6} for the presented basis size is 52. A systematic study of convergence with respect to the grid range, grid points N and numbers of single particle functions n has been carried out. The converged energy levels are given in Table II.

The levels are easily labeled by comparison with the harmonic frequencies, ω, obtained on our surface. We also report for comparison the harmonic frequencies from an earlier study, calculated at lower *ab initio* level than used for the present PES.[64] All vibrations are modeled reasonably well by the harmonic representation with the largest deviation of 31 cm^{-1} being observed for the antisymmetric stretching modes. The harmonic frequencies are between 1% and 2% higher than the accurately computed fundamentals, which indicates a fairly moderate anharmonicity of the PES. The only known experimental value of 1356.2 cm^{-1} for the e' asymmetric stretching vibration was obtained in a Ne matrix and is in excellent agreement with the frequency of 1352.9 cm^{-1} computed in the present work.[89]

TABLE II. Ground state energy with respect to the bottom of the potential energy surface and excitation energies for the first six vibrational states of NO_3^- in cm^{-1}. The harmonic frequencies, ω, obtained on our surface as well as the ones of Ref. 64 are also given.

Level	Description	E	ω	ω from Ref. 64
1	Ground state	3038		
2	Antisym bending	703	712	712
4	Antisym bending	703	712	712
5	Umbrella	845	857	843
6	Sym stretching	1040	1061	1073
6	Antisym stretching	1353	1384	1466
7	Antisym stretching	1353	1384	1466

The main purpose of the newly developed anion surface is to determine the initial state for the simulation of the photodetachment experiment. For this reason, no attempt has been made to compute higher vibrational states of NO_3^- so far.

B. PESs and dynamics of the $^2E''$ state of the NO_3 radical

1. Potential energy surfaces

For the investigation of our main target, the $^2E''$ state of the NO_3 radical, we first need to determine and develop the diabatic PESs. This state is a challenging test case for our method for two reasons. First of all, the Jahn-Teller coupling is rather strong but not strong enough to wipe out well resolved spectroscopic features entirely. Thus, the computed spectrum is extremely sensitive to the complicated details of the PESs. Second, the dissociation channel leading to NO_2 $(^2A_1)$ + O (^3P) is found at very low energy, only about 1 eV above the conical intersection for the ground state equilibrium geometry. This introduces extremely strong anharmonicity, which needs to be handled properly because the width of the experimental photodetachment spectrum of roughly 0.9 eV indicates that regions far into the dissociation channel are probably sampled by the wave-packet. This latter point also explains why a much larger region of the nuclear configuration space needs to be sampled and represented compared to the anion system.

The data acquisition followed a similar scheme to that for the anion. MRCI calculations were carried out for a large number of cuts through the PESs along random vectors. Most of the scans along these random cuts were concentrated in the region of the potential wells. Additional cuts were computed in which one N–O bond was stretched into the asymptotic region in order to obtain sufficient data to represent the lowest dissociation channel. The data acquisition and fitting was split in two steps utilizing symmetry. The majority of data was determined for planar geometries because all low-lying electronic states of NO_3 have planar equilibrium geometries. Furthermore, there is no additional coupling to the nearby ground state or second excited state as long as the system remains planar. We obtained 248 of the 318 potential parameters which are purely based on data points for planar geometries, while only 70 parameters depend on all six coordinates, including the umbrella motion. Energy data for roughly 10 000 geometry points were computed by MRCI *ab initio* calculations of which 1700 geometries included distortions out of the molecular plane. The distortions along the umbrella coordinate were limited to at most 10° because this motion induces couplings to the nearby $^2A_2'$ and $^2E'$ states, which cannot be accounted for in the present isolated model for the $^2E''$ state. These interactions will be included in a forthcoming study of all these low-lying states in an extended diabatic model. Below distortions of 10° the coupling effects are visible but small enough to be ignored for the time being. However, the effect of the ignored couplings becomes visible in the fitting errors of the 5D and 6D subsets of data. The rms error for all planar data is only 25 cm^{-1} for all points with energies below 1 eV above the origin (conical intersection obtained for the ground state equilibrium geometry). By contrast, the rms error for the 6D data is 125 cm^{-1} and this slightly increased deviation is mainly due to the missing couplings with excluded electronic states. These errors by themselves must not be over-interpreted because they only refer to the representation of the data in the fitting basis while the full 6D nuclear configuration space is heavily undersampled. Therefore, the convergence of the fit with respect to the data basis must be tested. To this means, *ab initio* energies at additional 1615 random geometries have been computed, which were not used in the fitting procedure, and the corresponding rms error has been determined. The resulting number is in almost perfect agreement with the fitting rms error, meaning that the final PESs fit presented here is converged and reliably represents the physically relevant regions. One further test of the quality of the fitted model is carried out by analysis and comparison of the equilibrium geometries computed at both the *ab initio* level and on the fitted surfaces. The equilibrium geometry is not contained in the fitting basis and thus the fit is not biased. The lower sheet of the adiabatic PESs shows three equivalent planar minima with an energy 0.398 eV below the reference energy at the conical intersection. The equilibrium geometries show one long N–O bond of 2.6781 bohrs and two short N–O distances of 2.2801 bohrs. The angle between the two short N–O bonds is 130.4°. By comparison, the *ab initio* geometry optimization yields one long N–O bond of 2.6746 bohrs, two short N–O distances of 2.2805 bohrs, and an angle of 130.3°. The *ab initio* energy of the minimum is found 0.395 eV below the reference point and thus is about 24 cm^{-1} above the one from the model. All above numbers are in very good agreement and the energy deviation is very similar to the obtained fitting rms. These results demonstrate the power of the presented model to fit and represent such a complicated system with high accuracy. The obtained diabatic PESs were used further for the investigation of the excited states dynamics and photodetachment spectrum. FORTRAN routines encoding this model and the corresponding parameters are available from the authors on request.

Before the dynamics is discussed, we consider the features of the obtained PESs. In Fig. 2 the two sheets of the

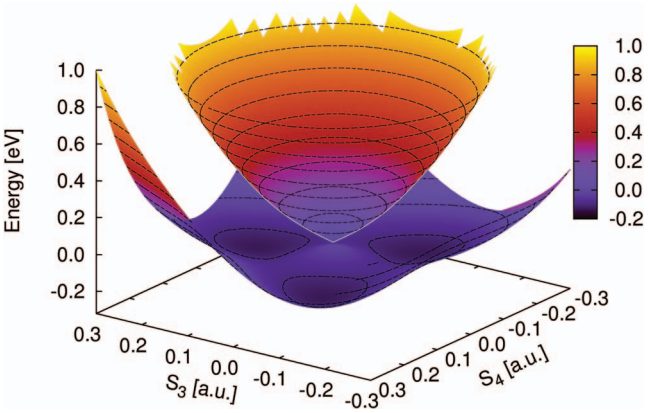

FIG. 2. Adiabatic PESs of the two sheets of the $^2E''$ state depending on the x and y component of the e' stretch coordinate, s_3 and s_4. The contour lines show energy levels between −0.1 and 0.9 eV with 0.1 eV spacing and the 0.0 eV level coinciding with the touching point of the conical intersection.

adiabatic PESs are shown as a function of a set of symmetrised asymmetric stretch coordinates s_3 and s_4 transforming as e'. These coordinates are of the form given in Eqs. (7c) and (7d), except that untransformed displacements of the N–O distances are used here as primitive coordinates.

The choice of symmetrised coordinates allows to visualize the intrinsic threefold symmetry of the system, which is properly represented by the diabatic model. This is reflected by the three equivalent minima, visible on the lower adiabatic sheet, which are connected by three equivalent transition states between the wells. The conical intersection is clearly seen at the origin of the plot where the upper conical sheet touches the lower sheet. A sensitive test of the proper symmetry of the PESs is to rotate the vector (s_3, s_4) by $\frac{2\pi}{3}$ or $\frac{4\pi}{3}$ and check the invariance of the adiabatic energies. This test proves that the method to generate the coupled PESs proposed in the present work yields the correct symmetry properties by construction. The invariance of the adiabatic nuclear wave function, however, would require a rotation by 4π due to the Berry or geometrical phase induced by the presence of the conical intersection.

It also may be of interest to have a look at the diabatic PESs corresponding to the adiabatic PESs discussed above. A representation of the two diagonal elements of the diabatic model, depending on the two coordinates s_3 and s_4, is given in Fig. 3. At first glance it is obvious that the two PESs intersect along a line where $s_3 = 0$ and that the two sheets do not display the threefold symmetry. Like the adiabatic PESs, these two functions are symmetric with respect to the $s_4 = 0$ line and unsymmetric with respect to the $s_3 = 0$ line. This is the proper behaviour, indeed, and corresponds to diabatic nuclear wave functions with the correct symmetry properties. After transformation into the adiabatic representation the PESs do reflect the global threefold symmetry of the system.

The asymptotic behaviour for the reactive channels of the adiabatic PESs is displayed in Fig. 4. In this case the plotting coordinates are two of the three equivalent true N–O bond distances. The remaining coordinates are frozen at the equilibrium values of the $^2A_2'$ ground state of neutral NO_3.

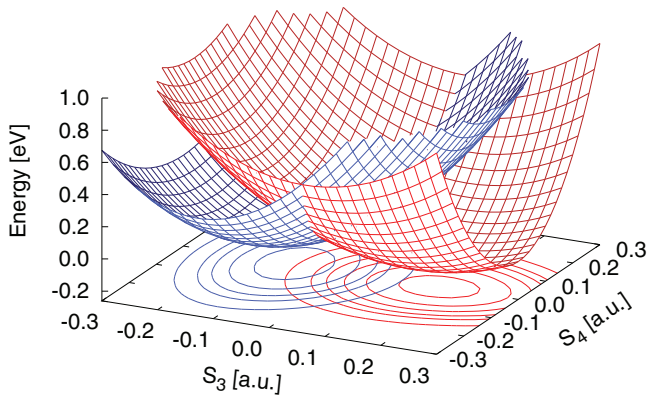

FIG. 3. Intersecting diabatic PESs corresponding to the $^2E''$ state depending on the x and y components of the e' stretch coordinate, s_3 and s_4, respectively. The contour lines show energy levels of 0.2 eV and below with 0.05 eV spacing.

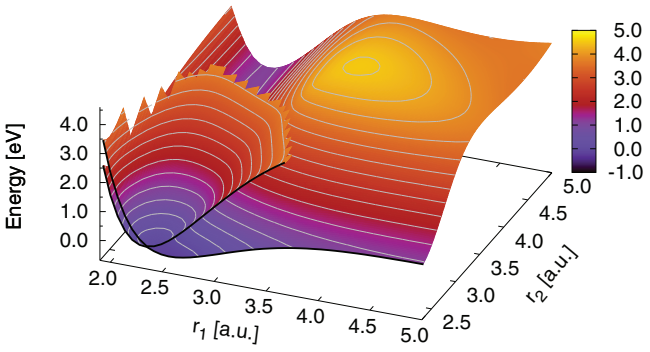

FIG. 4. Adiabatic PESs of the two sheets of the $^2E''$ state depending on the two N–O bond distances r_1 and r_2.

The conical intersection between the two adiabatic PESs is seen at the point where $r_1 = r_2 = r_e$ with a ground state equilibrium distance r_e of 2.344 a.u. The above mentioned low dissociation energy on the lower adiabatic sheet is immediately obvious from Fig. 4. In fact, the true exit channel is even slightly lower because in this 2D plot the relaxation of the NO_2 fragment is not accounted for. The bottom of the reaction channel is represented very accurately by the current diabatic model when compared to the underlying *ab initio* MRCI calculations. By contrast, the representation of the reactive channel $NO_3 \rightarrow NO + O + O$, which is seen on the diagonal of the plot, is only very approximate because no fitting data was used along this channel. This is justified by the fact that this region plays no role in the dynamics of interest because it is energetically inaccessible. The upper adiabatic sheet shows a behaviour very similar to that of the lower sheet but leading to an excited state exit channel at much higher energy. It is already known from our earlier calculations that this leads to additional intersections with the PESs for the $^2E'$ second excited state and may be important for the photodissociation dynamics.[59] This will be subject of further studies in which our diabatic model will be extended by including the other low-lying electronic states.

2. Multisurface dynamics

The coupled surfaces are used to compute the photoelectron detachment spectrum of NO_3^-. A vertical transition from the vibrational ground state of NO_3^- onto a 50-50 mixing of the diabatic surfaces of the radical is assumed to prepare an initial wave-packet. This wave-packet is then propagated for 200 fs from which the autocorrelation function is extracted. A smooth damping of the autocorrelation function is used after 180 fs before performing a Fourier transformation to obtain the spectrum.

The obtained theoretical photodetachment spectrum is presented together with the experimental data in Fig. 5. Because of the lack of size extensivity of the MRCI *ab initio* method, the computed absolute energies of NO_3^- and NO_3 cannot be compared directly. This means that no accurate absolute line positions can be computed for the electron detachment. However, this does not affect the relative line positions of the spectrum. Thus, we present a theoretical spectrum

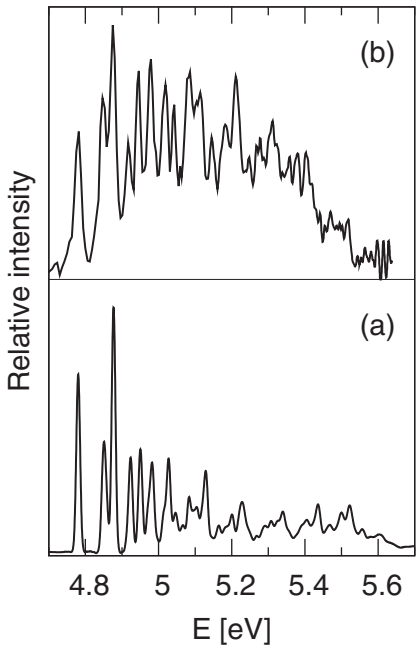

FIG. 5. Theoretical photodetachment spectrum in panel (a) compared with the experimental spectrum of Ref. 68 in arbitrary intensity units. The theoretical spectrum is adjusted in energy to match the first peak of the experimental one.

which is shifted such that the first peak is in agreement with the experimental one. In the theoretical spectrum, the width of the lines depends on the choice of the damping time of the autocorrelation function. With the 180 fs value used here, the overall shape of the spectrum as well as the width of the individual peaks as shown in Fig. 6 can be easily compared with the experimental data. The basis set used for the wavepacket representation is given in Table I. This quite large basis ensures that the presented spectrum is converged. The propagation time of 200 fs is chosen sufficiently long to remove artificial oscillations in the resulting spectrum. As seen in Fig. 5, the energy range of the spectrum, roughly 1 eV, is properly reproduced by the theoretical model. Both the experimental and the theoretical spectrum show a more structured shape at the low energy part while at higher energies the spectrum becomes congested and lines are not well resolved. For the low energy part the structure is reproduced in excellent agreement with experiment by our model as shown in Fig. 6. When compared to the less elaborate model of Ref. 64, the present model reproduces the spectrum with significantly better accuracy. In particular, the second and third peaks are no longer superimposed as in the preliminary model (see Fig. 5 of Ref. 64). For the less resolved higher energy part of the spectrum (above 5.2 eV) the agreement with experiment does not seem as excellent. This may be due to two different effects. One could be that the quality of the *ab initio* data and therefore the PESs slightly deteriorates for higher energies, giving rise to slightly wrong energy levels. Another reason could be deviations in the line intensities and the resolution of both experimental spectrum and theoretical simulation. The time-independent calculations of the spectrum presented in Ref. 64 showed that for higher energies the observed peaks are composed of a large number of unresolved detachment lines. The resulting spectral envelope is probably rather sensitive to small deviations of the single line positions and intensities in both experiment and simulation. Furthermore, a major problem with the intensities is obvious at first glance from Fig. 5. While the base line of the theoretical simulation is almost flat, the experimental spectrum seems to be superimposed with a Gaussian shaped background, which results in strongly enhanced intensities in the mid-range of the spectrum. It is not clear what the origin of this behaviour is. Too low intensities at higher energies are easily explained by Wigner's well-known threshold law but enhanced intensities as observed here must be due to a different reason.

During the propagation time of 200 fs, the diabatic populations stay around 0.50 ± 0.05 for both states. However, these populations have little physical meaning and more relevant are the adiabatic populations. The numerical convergence of these is quite difficult to achieve and forced us to use the large basis set presented in Table I. In Fig. 7 we present the evolution of the population on the lower adiabatic PES, while the population on the upper adiabatic PES corresponds to the complement to one. At the initial time,

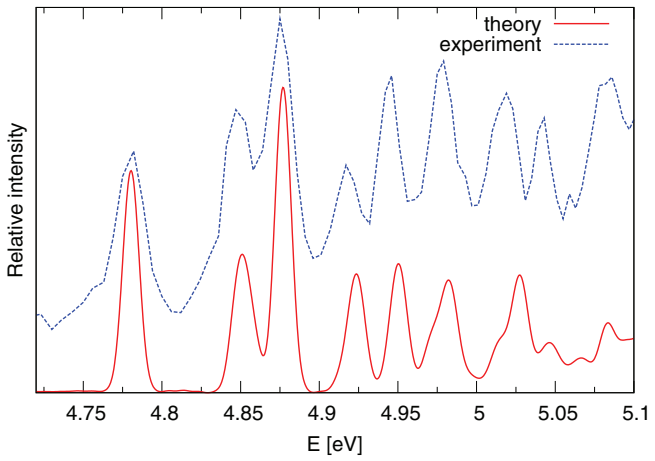

FIG. 6. Same as Fig. 5 focusing on the low energy part of the spectra. The experimental spectrum is vertically shifted for better reading of the figure.

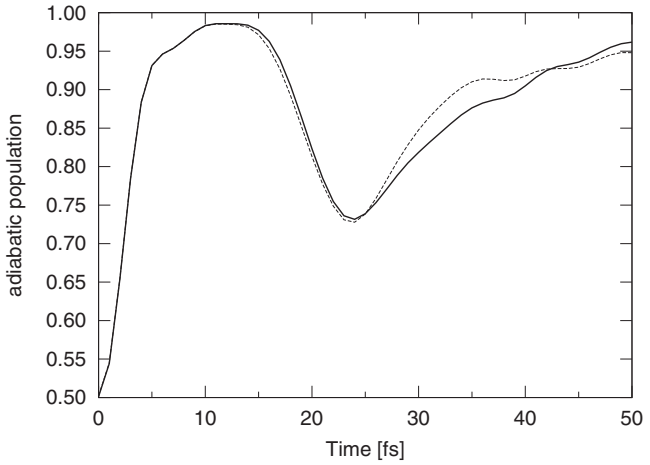

FIG. 7. Adiabatic population on the lower adiabatic PES sheet as a function of time in fs. The full line corresponds to the basis size of Table I while the dashed line presents the results with a slightly smaller basis (see text).

the populations on the two adiabatic PESs are both 0.5. Within 10 fs, the non-adiabatic effects induce a nearly complete transfer of the population to the lower PES sheet. After 25 fs, a maximum of back transfer is observed with a population of 0.75 on the lower sheet before another transfer towards the ground state sets in. At 50 fs, a second maximum of the adiabatic population on the ground state PES is observed. The dashed line in Fig. 7 corresponds to a calculation with a smaller basis set, lowering the five $n = 14$ to $n = 12$, and allows us to present the degree of convergence of the results. The largest difference between the two calculations occurs at 33 fs with a value of 0.036, thus corresponding to a 4% relative error. A more detailed analysis of the adiabatic population dynamics based of the analysis of the wave-packet is not straightforward due to the rather non-intuitive definition of the stereographic projection coordinates used here for the wave packet propagations. Since in the present work the focus is more on the development of accurate PESs, such an analysis will be given in a forthcoming study.

IV. CONCLUSIONS

A new model has been developed to represent full-dimensional coupled PESs for typical Jahn-Teller systems with high accuracy. This model allows for the proper inclusion of dissociative regions and is suitable for quantum dynamics calculations. The new approach is applied to the $^2E''$ excited state of NO_3 for the first time and results in PESs of unprecedented quality.

This model is based on a diabatic potential matrix and on the expansion of the corresponding matrix elements in parametrized symmetry polynomials of symmetrized coordinates. These polynomials and coordinates have the appropriate transformation properties under all symmetry operations of the molecular point group, D_{3h} in the present case. In contrast to previous studies, all symmetry-allowed multi-coordinate terms up to at least 6th order are included in the present model. Besides this expansion to higher orders, a key to represent reactive channels and to achieve the high accuracy we aim for is the choice of suitable coordinates. Due to the polynomial expansion, the dissociative channels cannot be accounted for by linear distance coordinates. Therefore, distances must be transformed appropriately. We found that the widely used inverse pairwise distances are not optimal for this purpose and instead propose to use both the very flexible tunable Morse coordinates developed by us and scaled angular coordinates. We tested that our choice of coordinate set containing both transformed distances and angles is superior to the coordinate set consisting of all inverse pairwise distances. This might be a fairly general observation because simple stretching and bending motions become strongly correlated when expressed in all pairwise distances.

An important aspect of the present work is how to determine the optimal free parameters of the diabatic potential model. First of all, the PESs developed here are entirely based on high-level *ab initio* CCSD(T) and MRCI calculations without any adjustment to experimental data. Only the energy difference between the anion and the neutral system is taken from the experiment since it cannot be computed reliably with present electronic structure methods. The free parameters are obtained by non-linear least-squares fitting with respect to adiabatic *ab initio* energies for a large number of geometries. They are available upon request to the authors. In order to avoid an overly biased selection of data points of the heavily undersampled 6D nuclear configuration space, a stochastic approach is used that is based on cuts along random vectors through the 6D PESs along which the adiabatic energies are determined. It is ensured that the physically relevant regions of the nuclear configuration space are sufficiently sampled by choosing the origin and the allowed ranges for each of the six components of random displacement vectors defining the directions of the cuts. Thus, the remaining and necessary bias in the selection of data points is the choice of relevant regions and the range of scanning. The convergence of the fitted PESs with respect to the data basis is ensured by testing the deviations between random data not used during the fitting procedure and the PESs. The intended exclusion of physically irrelevant data points from the fitting basis often leads to the problem that the PES model yields artificially low energies in the omitted regions. A new approach is proposed how to avoid this issue. The diabatic potential model is split into a reference and a correction model of which the first represents the PESs roughly even in the omitted regions and the latter corrects this rough estimate with high accuracy in the physically relevant areas. In the final model, the correction is switched off wherever the energies of the full model would fall artificially far below the energies of the reference model. The resulting PESs are unchanged and very accurate in the relevant regions and roughly but sufficiently reasonably represented in the otherwise problematic areas.

An extremely sensitive test for the quality of the presented diabatic potential model is its use in quantum dynamics calculations and in particular for the simulation of the experimentally known photodetachment spectrum of NO_3^-. We present the results of full-dimensional wave-packet propagations using the developed full dimensional two-sheeted coupled potential surface and the MCTDH method. The peak positions of the low energy part of the simulated spectrum are in almost perfect agreement with experiment. At higher energies, this agreement deteriorates somewhat. Significant deviations are found for the peak intensities over the entire range of the spectrum. It appears like there is a broad background in the experimental spectrum, which is not reproduced in the simulation. The physical origin of the differing intensities is presently unclear and may also contribute to the deviations of peak positions in the higher energy part of the spectrum. In fact, the discernible peaks at higher energies do not correspond to single vibronic levels but are superpositions of detachments to many closely spaced levels. Thus, the actual peak position and intensity depends on the minute details of level energies and detachment intensities for each of a huge number of vibronic states. It seems unlikely that the underlying *ab initio* data are of sufficient accuracy to reproduce the chaotic part of the spectrum much better. Presently, it cannot be decided whether shortcomings of the electronic structure

methods or the diabatic model are responsible for the deviations. At least for low energies the quality of the diabatic model and the underlying *ab initio* data is demonstrated by the dynamical simulations.

Finally, we also report results for the nonadiabatic population dynamics between the two PES sheets of the $^2E''$ state after the initial detachment of the electron modeled by a simple vertical excitation from the anion to the radical surfaces. It is observed that the initial population of the wave-packet on the upper sheet rapidly and almost completely decays to the lower sheet within 10 fs. However, a significant re-population of the upper sheet takes place within the next roughly 10 to 15 fs before a second and slower decay sets in. This re-population may explain, at least to some extent, why the detachment spectrum is so hard to simulate and why it requires such an elaborate and accurate diabatic potential model: The wave-packet stays in the Condon region even after relatively long propagation time, experiencing fairly strong nonadiabatic couplings. During the same time it samples extended areas of the PESs around the Condon region. Both give rise to very complex behaviour which is very sensitive to the details of the PESs and the couplings.

The present study demonstrates that the developed diabatic potential model is capable of yielding very good PESs for studying the quantum dynamics of a complicated and strongly coupled system like NO_3. However, the $^2E''$ state investigated here is only one of at least three relevant states to understand the spectroscopy and photochemistry of NO_3. Therefore, this study needs to be extended to a diabatic potential model including the $^2A_2'$ and $^2E'$ states as well. Corresponding work is currently in progress. A more detailed investigation of the effects of the Jahn-Teller coupling within the $^2E''$ state on the quantum dynamics is also underway. Several aspects of the presented model development can be transferred to other strongly coupled molecular systems and to the generation of highly accurate PESs in general. In particular, an extension to larger and less symmetric molecules will be of great interest.

ACKNOWLEDGMENTS

The authors acknowledge the generous financial support via the UFA-DFH organization. This work has also been supported by the University of Rennes 1 via an invited professorship of W.E. Uwe Manthe and Robert Wodraszka are warmly acknowledged for fruitful discussions. The authors thank Robert Wodraszka for providing his source code for the kinetic operator term. We wish to thank Daniel M. Neumark and Madeline Elkins for their archaeological endeavour of digging out the original experimental data of the photodetachment spectrum and kindly sending it to us for comparison.

APPENDIX: SYMMETRY POLYNOMIALS AND DIABATIC MATRIX ELEMENTS

In the following, the general form of the matrix elements of the diabatic potential matrix are given. Each matrix element can be expanded in the proper symmetry polynomials in the corresponding symmetry coordinates. Problematic are only terms involving the degenerate e' coordinates $e_i' = (x_i, y_i);\ i = 1, 2$. Expansion terms for the $\mathcal{V}$, $\mathcal{W}$, and $\mathcal{Z}$ functions in Eq. (9) involving only one of the two sets of e' coordinates have been published in Refs. 50, 51. In the present work, we also include all mode-mode couplings among the two sets of e' coordinates. The corresponding expansion terms are given below. To derive these terms by the method described in Refs. 50, 51 one first transforms the two sets of degenerate coordinates x_1, y_1 and x_2, y_2 into the complex plane by

$$Q_{i+} = \frac{1}{\sqrt{2}}(x_i + iy_i) \quad \text{and} \quad Q_{i-} = \frac{1}{\sqrt{2}}(x_i - iy_i). \tag{A1}$$

In the complex plane, the critical symmetry operator $\widehat{C}_3$ can be applied easily and one obtains

$$\widehat{C}_3\ Q_{i+} = e^{+2\pi i/3}\ Q_{i+} \quad \text{and} \quad \widehat{C}_3\ Q_{i-} = e^{-2\pi i/3}\ Q_{i-}. \tag{A2}$$

A corresponding transformation to the complex plane is carried out for the two components of the E state and yields the respective eigenvalues when $\widehat{C}_3$ is applied. The application of $\widehat{C}_3$ on each term $|\Psi_k\rangle H_{kl}^d \langle\Psi_l|$ of the spectral representation of the Hamiltonian must yield an eigenvalue of 1 since $\widehat{H}$ must be invariant under any symmetry transformation. The matrix elements H_{kl}^d of the diabatic Hamiltonian are expanded as polynomials in the complex coordinates and only terms invariant under the $\widehat{C}_3$ transformation are retained. To this end one may utilize Table I of Ref. 51, in which the surviving terms are listed, and replace the products $Q_+^p Q_-^q$ by all unique combinations of $Q_{1+}^{p_1} Q_{2+}^{p_2} Q_{1-}^{q_1} Q_{2-}^{p_2}$ with $p_1 + p_2 = p$ $(p_1 \geq p_2)$ and $q_1 + q_2 = q$ $(q_1 \geq q_2)$. The complex diabatic Hamiltonian is set up for each order $p + q$ and each unique combination (p_1, p_2, q_1, q_2) and then back-transformed into the real coordinate plane. This yields the real diabatic Hamiltonian matrices of Eq. (9) with the elements $v_{ee}^{(n,m)}$, $w_{ee}^{(n,m)}$, and $z_{ee}^{(n,m)}$ $(n = p + q)$:

$$v_{ee}^{(2,1)} = 2(x_1x_2 + y_1y_2), \tag{A3a}$$

$$v_{ee}^{(3,1)} = 2\left(x_1x_2^2 - x_1y_2^2 - 2x_2y_1y_2\right), \tag{A3b}$$

$$v_{ee}^{(3,2)} = 2\left(x_1^2x_2 - x_2y_1^2 - 2x_1y_1y_2\right), \tag{A3c}$$

$$v_{ee}^{(4,1)} = 2\left(x_1^2x_2^2 - x_1^2y_2^2 - x_2^2y_1^2 + y_1^2y_2^2 + 4x_1x_2y_1y_2\right), \tag{A3d}$$

$$v_{ee}^{(4,2)} = 2\left(x_1^3x_2 + x_1^2y_1y_2 + x_1x_2y_1^2 + y_1^3y_2\right), \tag{A3e}$$

$$v_{ee}^{(4,3)} = 2\left(x_2^3x_1 + x_1x_2y_2^2 + x_2^2y_1y_2 + y_2^3y_1\right), \tag{A3f}$$

$$v_{ee}^{(4,4)} = x_1^2x_2^2 + x_1^2y_2^2 + x_2^2y_1^2 + y_1^2y_2^2, \tag{A3g}$$

$$v_{ee}^{(5,1)} = x_1y_2^4 - 4x_2y_1y_2^3 - 6x_1x_2^2y_2^2 + 4x_2^3y_1y_2 + x_1x_2^4, \tag{A3h}$$

$$v_{ee}^{(5,2)} = \left(y_2^2 + x_2^2\right)\left(x_1y_2^2 + 2x_2y_1y_2 - x_1x_2^2\right), \tag{A3i}$$

$$v_{ee}^{(5,3)} = \left(y_1^2 + x_1^2\right)\left(x_1y_2^2 + 2x_2y_1y_2 - x_1x_2^2\right), \tag{A3j}$$

$$v_{ee}^{(5,4)} = x_2\left(y_1^2 + x_1^2\right)\left(3y_2^2 - x_2^2\right), \tag{A3k}$$

$$v_{ee}^{(5,5)} = \left(2x_1y_1y_2 + x_2y_1^2 - x_1^2x_2\right)\left(y_2^2 + x_2^2\right), \tag{A3l}$$

$$v_{ee}^{(5,6)} = x_1\left(3y_1^2 - x_1^2\right)\left(y_2^2 + x_2^2\right), \tag{A3m}$$

$$v_{ee}^{(5,7)} = 4x_1y_1^3y_2 - 4x_1^3y_1y_2 - x_2y_1^4 + 6x_1^2x_2y_1^2 - x_1^4x_2, \tag{A3n}$$

$$v_{ee}^{(5,8)} = \left(y_1^2 + x_1^2\right)\left(2x_1y_1y_2 + x_2y_1^2 - x_1^2x_2\right), \tag{A3o}$$

$$v_{ee}^{(6,1)} = \left(y_1y_2^5 - 5x_1x_2y_2^4 - 10x_2^2y_1y_2^3 + 10x_1x_2^3y_2^2 + 5x_2^4y_1y_2 - x_1x_2^5\right), \tag{A3p}$$

$$v_{ee}^{(6,2)} = \left(y_1y_2^2 - x_1y_2^2 - 2x_2y_1y_2 - 2x_1x_2y_2 - x_2^2y_1 + x_1x_2^2\right) \times \left(y_1y_2^2 + x_1y_2^2 + 2x_2y_1y_2 - 2x_1x_2y_2 - x_2^2y_1 - x_1x_2^2\right), \tag{A3q}$$

$$v_{ee}^{(6,3)} = \left(y_1y_2 - x_1x_2\right)\left(y_1^2y_2^2 - 3x_1^2y_2^2 - 8x_1x_2y_1y_2 - 3x_2^2y_1^2 + x_1^2x_2^2\right), \tag{A3r}$$

$$v_{ee}^{(6,4)} = \left(y_1^2y_2 - 2x_1y_1y_2 - x_1^2y_2 - x_2y_1^2 - 2x_1x_2y_1 + x_1^2x_2\right) \times \left(y_1^2y_2 + 2x_1y_1y_2 - x_1^2y_2 + x_2y_1^2 - 2x_1x_2y_1 - x_1^2x_2\right), \tag{A3s}$$

$$v_{ee}^{(6,5)} = y_1^5y_2 - 10x_1^2y_1^3y_2 + 5x_1^4y_1y_2 - 5x_1x_2y_1^4 + 10x_1^3x_2y_1^2 - x_1^5x_2, \tag{A3t}$$

$$v_{ee}^{(6,6)} = (y_1y_2 + x_1x_2)\left(y_2^2 + x_2^2\right)^2, \tag{A3u}$$

$$v_{ee}^{(6,7)} = (y_1y_2 - x_1y_2 + x_2y_1 + x_1x_2)(y_1y_2 + x_1y_2 - x_2y_1 + x_1x_2)\left(y_2^2 + x_2^2\right), \tag{A3v}$$

$$v_{ee}^{(6,8)} = \left(y_1^2 + x_1^2\right)\left(y_2^2 + x_2^2\right)^2, \tag{A3w}$$

$$v_{ee}^{(6,9)} = (y_1y_2 + x_1x_2)\left(y_1^2y_2^2 - 3x_1^2y_2^2 + 8x_1x_2y_1y_2 - 3x_2^2y_1^2 + x_1^2x_2^2\right), \tag{A3x}$$

$$v_{ee}^{(6,10)} = \left(y_1^2 + x_1^2\right)(y_1y_2 + x_1x_2)\left(y_2^2 + x_2^2\right), \tag{A3aa}$$

$$v_{ee}^{(6,11)} = \left(y_1^2 + x_1^2\right)(y_1y_2 - x_1y_2 + x_2y_1 + x_1x_2) \times (y_1y_2 + x_1y_2 - x_2y_1 + x_1x_2), \tag{A3bb}$$

$$v_{ee}^{(6,12)} = \left(y_1^2 + x_1^2\right)^2\left(y_2^2 + x_2^2\right), \tag{A3cc}$$

$$v_{ee}^{(6,13)} = \left(y_1^2 + x_1^2\right)^2(y_1y_2 + x_1x_2). \tag{A3dd}$$

$$w_{ee}^{(2,1)} = x_1x_2 - y_1y_2, \tag{A4a}$$

$$w_{ee}^{(3,1)} = x_1^2x_2 + x_2y_1^2, \tag{A4b}$$

$$w_{ee}^{(3,2)} = x_1y_2^2 + x_1x_2^2, \tag{A4c}$$

$$w_{ee}^{(3,3)} = 2x_1y_1y_2 + x_1^2x_2 - x_2y_1^2, \tag{A4d}$$

$$w_{ee}^{(3,4)} = x_1x_2^2 + 2x_2y_1y_2 - x_1y_2^2, \tag{A4e}$$

$$w_{ee}^{(4,1)} = x_1^3x_2 - 3x_1^2y_1y_2 - 3x_1x_2y_1^2 + y_1^3y_2, \tag{A4f}$$

$$w_{ee}^{(4,2)} = x_1^2x_2^2 - x_1^2y_2^2 - x_2^2y_1^2 + y_1^2y_2^2 - 4x_1x_2y_1y_2, \tag{A4g}$$

$$w_{ee}^{(4,3)} = x_2^3x_1 - 3x_1x_2y_2^2 - 3x_2^2y_1y_2 + y_2^3y_1, \tag{A4h}$$

$$w_{ee}^{(4,4)} = x_1^3x_2 + 3x_1^2y_1y_2 - 3x_1x_2y_1^2 - y_1^3y_2, \tag{A4i}$$

$$w_{ee}^{(4,5)} = x_2^3x_1 - 3x_1x_2y_2^2 + 3x_2^2y_1y_2 - y_2^3y_1, \tag{A4j}$$

$$w_{ee}^{(4,6)} = x_1^3x_2 - x_1^2y_1y_2 + x_1x_2y_1^2 - y_1^3y_2, \tag{A4k}$$

$$w_{ee}^{(4,7)} = x_1^2x_2^2 + x_1^2y_2^2 - x_2^2y_1^2 - y_1^2y_2^2, \tag{A4l}$$

$$w_{ee}^{(4,8)} = x_1^2x_2^2 - x_1^2y_2^2 + x_2^2y_1^2 - y_1^2y_2^2, \tag{A4m}$$

$$w_{ee}^{(4,9)} = x_1x_2^3 + x_1x_2y_2^2 - x_2^2y_1y_2 - y_2^3y_1, \tag{A4n}$$

$$w_{ee}^{(5,1)} = x_1y_2^4 + 4x_2y_1y_2^3 - 6x_1x_2^2y_2^2 - 4x_2^3y_1y_2 + x_1x_2^4, \tag{A4o}$$

$$w_{ee}^{(5,2)} = 2x_1y_1y_2^3 + 3x_2y_1^2y_2^2 - 3x_1^2x_2y_2^2 - 6x_1x_2^2y_1y_2 - x_2^3y_1^2 + x_1^2x_2^3, \tag{A4p}$$

$$w_{ee}^{(5,3)} = 3x_1y_1^2y_2^2 - x_1^3y_2^2 + 2x_2y_1^3y_2 - 6x_1^2x_2y_1y_2 - 3x_1x_2^2y_1^2 + x_1^3x_2^2, \tag{A4q}$$

$$w_{ee}^{(5,4)} = 4x_1y_1^3y_2 - 4x_1^3y_1y_2 + x_2y_1^4 - 6x_1^2x_2y_1^2 + x_1^4x_2, \tag{A4r}$$

$$w_{ee}^{(5,5)} = -\left(y_2^2 + x_2^2\right)\left(x_1y_2^2 - 2x_2y_1y_2 - x_1x_2^2\right), \tag{A4s}$$

$$w_{ee}^{(5,6)} = x_1\left(y_2^2 + x_2^2\right)^2, \tag{A4t}$$

$$w_{ee}^{(5,7)} = -\left(2x_1y_1y_2^3 - 3x_2y_1^2y_2^2 + 3x_1^2x_2y_2^2 - 6x_1x_2^2y_1y_2 + x_2^3y_1^2 - x_1^2x_2^3\right), \tag{A4u}$$

$$w_{ee}^{(5,8)} = x_2\left(y_1^2 + x_1^2\right)\left(y_2^2 + x_2^2\right), \tag{A4v}$$

$$w_{ee}^{(5,9)} = -\left(y_1^2 + x_1^2\right)\left(x_1y_2^2 - 2x_2y_1y_2 - x_1x_2^2\right), \tag{A4w}$$

$$w_{ee}^{(5,10)} = x_1\left(y_1^2 + x_1^2\right)\left(y_2^2 + x_2^2\right), \tag{A4x}$$

$$w_{ee}^{(5,11)} = x_2\left(y_1^2 + x_1^2\right)^2, \tag{A4y}$$

$$w_{ee}^{(5,12)} = \left(y_1^2 + x_1^2\right)\left(2x_1y_1y_2 - x_2y_1^2 + x_1^2x_2\right), \tag{A4z}$$

$$w_{ee}^{(6,1)} = y_1y_2^5 + 5x_1x_2y_2^4 - 10x_2^2y_1y_2^3 - 10x_1x_2^3y_2^2 + 5x_2^4y_1y_2 + x_1x_2^5, \tag{A4aa}$$

$$w_{ee}^{(6,2)} = \left(y_2^2 + x_2^2\right)\left(y_1y_2^3 - 3x_1x_2y_2^2 - 3x_2^2y_1y_2 + x_1x_2^3\right), \tag{A4bb}$$

$$w_{ee}^{(6,3)} = \left(y_1^2 + x_1^2\right)\left(y_2^2 - 2x_2y_2 - x_2^2\right)\left(y_2^2 + 2x_2y_2 - x_2^2\right), \tag{A4cc}$$

$$w_{ee}^{(6,4)} = (y_1y_2 - x_1y_2 - x_2y_1 - x_1x_2)(y_1y_2 + x_1y_2 + x_2y_1 - x_1x_2)\left(y_2^2 + x_2^2\right), \tag{A4dd}$$

$$w_{ee}^{(6,5)} = \left(y_1^2 + x_1^2\right)\left(y_1y_2^3 - 3x_1x_2y_2^2 - 3x_2^2y_1y_2 + x_1x_2^3\right), \tag{A4ee}$$

$$w_{ee}^{(6,6)} = \left(y_1^3y_2 - 3x_1^2y_1y_2 - 3x_1x_2y_1^2 + x_1^3x_2\right)\left(y_2^2 + x_2^2\right), \tag{A4ff}$$

$$w_{ee}^{(6,7)} = \left(y_1^2 + x_1^2\right)(y_1y_2 - x_1y_2 - x_2y_1 - x_1x_2) \times (y_1y_2 + x_1y_2 + x_2y_1 - x_1x_2), \tag{A4gg}$$

$$w_{ee}^{(6,8)} = \left(y_1^2 - 2x_1y_1 - x_1^2\right)\left(y_1^2 + 2x_1y_1 - x_1^2\right)\left(y_2^2 + x_2^2\right), \tag{A4hh}$$

$$w_{ee}^{(6,9)} = \left(y_1^2 + x_1^2\right)\left(y_1^3y_2 - 3x_1^2y_1y_2 - 3x_1x_2y_1^2 + x_1^3x_2\right), \tag{A4ii}$$

$$w_{ee}^{(6,10)} = y_1^5y_2 - 10x_1^2y_1^3y_2 + 5x_1^4y_1y_2 + 5x_1x_2y_1^4 - 10x_1^3x_2y_1^2 + x_1^5x_2, \tag{A4jj}$$

$$w_{ee}^{(6,11)} = (y_1y_2 - x_1x_2)\left(y_2^2 + x_2^2\right)^2, \tag{A4kk}$$

$$w_{ee}^{(6,12)} = \left(y_2^2 + x_2^2\right)\left(y_1y_2^3 + 3x_1x_2y_2^2 - 3x_2^2y_1y_2 - x_1x_2^3\right), \tag{A4ll}$$

$$w_{ee}^{(6,13)} = \left(y_1^2 + x_1^2\right)(y_2 - x_2)(y_2 + x_2)\left(y_2^2 + x_2^2\right), \tag{A4mm}$$

$$w_{ee}^{(6,14)} = (y_1 - x_1)(y_1 + x_1)\left(y_2^2 + x_2^2\right)^2, \tag{A4nn}$$

$$w_{ee}^{(6,15)} = \left(y_1y_2^2 - x_1y_2^2 + 2x_2y_1y_2 + 2x_1x_2y_2 - x_2^2y_1 + x_1x_2^2\right) \times \left(y_1y_2^2 + x_1y_2^2 - 2x_2y_1y_2 + 2x_1x_2y_2 - x_2^2y_1 - x_1x_2^2\right), \tag{A4oo}$$

$$w_{ee}^{(6,16)} = \left(y_1^3y_2 - 3x_1^2y_1y_2 + 3x_1x_2y_1^2 - x_1^3x_2\right)\left(y_2^2 + x_2^2\right), \tag{A4pp}$$

$$w_{ee}^{(6,17)} = \left(y_1^2 + x_1^2\right)(y_1y_2 - x_1x_2)\left(y_2^2 + x_2^2\right), \tag{A4qq}$$

$$w_{ee}^{(6,18)} = \left(y_1^2 + x_1^2\right)\left(y_1y_2^3 + 3x_1x_2y_2^2 - 3x_2^2y_1y_2 - x_1x_2^3\right), \tag{A4rr}$$

$$w_{ee}^{(6,19)} = \left(y_1^2y_2 - 2x_1y_1y_2 - x_1^2y_2 + x_2y_1^2 + 2x_1x_2y_1 - x_1^2x_2\right) \times \left(y_1^2y_2 + 2x_1y_1y_2 - x_1^2y_2 - x_2y_1^2 + 2x_1x_2y_1 + x_1^2x_2\right), \tag{A4ss}$$

$$w_{ee}^{(6,20)} = (y_1 - x_1)(y_1 + x_1)\left(y_1^2 + x_1^2\right)\left(y_2^2 + x_2^2\right), \tag{A4tt}$$

$$w_{ee}^{(6,21)} = \left(y_1^2 + x_1^2\right)^2(y_2 - x_2)(y_2 + x_2), \tag{A4uu}$$

$$w_{ee}^{(6,22)} = \left(y_1^2 + x_1^2\right)\left(y_1^3y_2 - 3x_1^2y_1y_2 + 3x_1x_2y_1^2 - x_1^3x_2\right), \tag{A4vv}$$

$$w_{ee}^{(6,23)} = \left(y_1^2 + x_1^2\right)^2(y_1y_2 - x_1x_2). \tag{A4ww}$$

$$z_{ee}^{(2,1)} = -x_1y_2 - x_2y_1, \tag{A5a}$$

$$z_{ee}^{(3,1)} = y_1^2y_2 + x_1^2y_2, \tag{A5b}$$

$$z_{ee}^{(3,2)} = y_1y_2^2 + x_2^2y_1, \tag{A5c}$$

$$z_{ee}^{(3,3)} = y_1^2y_2 + 2x_1x_2y_1 - x_1^2y_2, \tag{A5d}$$

$$z_{ee}^{(3,4)} = y_2^2y_1 + 2x_1x_2y_2 - x_2^2y_1, \tag{A5e}$$

$$z_{ee}^{(4,1)} = x_1^3y_2 + 3x_1^2x_2y_1 - 3x_1y_1^2y_2 - x_2y_1^3, \tag{A5f}$$

$$z_{ee}^{(4,2)} = 2x_1^2x_2y_2 + 2x_1x_2^2y_1 - 2x_1y_1y_2^2 - 2x_2y_1^2y_2, \tag{A5g}$$

$$z_{ee}^{(4,3)} = x_2^3y_1 + 3x_1x_2^2y_2 - 3x_2y_1y_2^2 - x_1y_2^3, \tag{A5h}$$

$$z_{ee}^{(4,4)} = x_1^3y_2 - 3x_1^2x_2y_1 - 3x_1y_1^2y_2 + x_2y_1^3, \tag{A5i}$$

$$z_{ee}^{(4,5)} = x_2^3y_1 - 3x_1x_2^2y_2 - 3x_2y_1y_2^2 + x_1y_2^3, \tag{A5j}$$

$$z_{ee}^{(4,6)} = -x_1^3y_2 - x_1^2x_2y_1 - x_1y_1^2y_2 - x_2y_1^3, \tag{A5k}$$

$$z_{ee}^{(4,7)} = -2x_1x_2^2y_1 - 2x_1y_1y_2^2, \tag{A5l}$$

$$z_{ee}^{(4,8)} = -2x_1^2x_2y_2 - 2x_2y_1^2y_2, \tag{A5m}$$

$$z_{ee}^{(4,9)} = -y_2^3x_1 - x_1x_2^2y_2 - x_2y_1y_2^2 - y_1x_2^3, \tag{A5n}$$

$$z_{ee}^{(5,1)} = -\left(y_1y_2^4 - 4x_1x_2y_2^3 - 6x_2^2y_1y_2^2 + 4x_1x_2^3y_2 + x_2^4y_1\right), \tag{A5o}$$

$$z_{ee}^{(5,2)} = -\left(y_1^2y_2^3 - x_1^2y_2^3 - 6x_1x_2y_1y_2^2 - 3x_2^2y_1^2y_2 + 3x_1^2x_2^2y_2 + 2x_1x_2^3y_1\right), \tag{A5p}$$

$$z_{ee}^{(5,3)} = -\left(y_1^3y_2^2 - 3x_1^2y_1y_2^2 - 6x_1x_2y_1^2y_2 + 2x_1^3x_2y_2 - x_2^2y_1^3 + 3x_1^2x_2^2y_1\right), \tag{A5q}$$

$$z_{ee}^{(5,4)} = -\left(y_1^4y_2 - 6x_1^2y_1^2y_2 + x_1^4y_2 - 4x_1x_2y_1^3 + 4x_1^3x_2y_1\right), \tag{A5r}$$

$$z_{ee}^{(5,5)} = \left(y_2^2 + x_2^2\right)\left(y_1y_2^2 + 2x_1x_2y_2 - x_2^2y_1\right), \tag{A5s}$$

$$z_{ee}^{(5,6)} = y_1\left(y_2^2 + x_2^2\right)^2, \tag{A5t}$$

$$z_{ee}^{(5,7)} = y_1^2y_2^3 - x_1^2y_2^3 + 6x_1x_2y_1y_2^2 - 3x_2^2y_1^2y_2 + 3x_1^2x_2^2y_2 - 2x_1x_2^3y_1, \tag{A5u}$$

$$z_{ee}^{(5,8)} = \left(y_1^2 + x_1^2\right)y_2\left(y_2^2 + x_2^2\right), \tag{A5v}$$

$$z_{ee}^{(5,9)} = \left(y_1^2 + x_1^2\right)\left(y_1 y_2^2 + 2x_1 x_2 y_2 - x_2^2 y_1\right), \tag{A5w}$$

$$z_{ee}^{(5,10)} = y_1\left(y_1^2 + x_1^2\right)\left(y_2^2 + x_2^2\right), \tag{A5x}$$

$$z_{ee}^{(5,11)} = \left(y_1^2 + x_1^2\right)^2 y_2, \tag{A5y}$$

$$z_{ee}^{(5,12)} = \left(y_1^2 + x_1^2\right)\left(y_1^2 y_2 - x_1^2 y_2 + 2x_1 x_2 y_1\right), \tag{A5z}$$

$$\begin{aligned} z_{ee}^{(6,1)} = {} & x_1 y_2^5 - 5x_2 y_1 y_2^4 - 10x_1 x_2^2 y_2^3 \\ & + 10x_2^3 y_1 y_2^2 + 5x_1 x_2^4 y_2 - x_2^5 y_1, \end{aligned} \tag{A5aa}$$

$$z_{ee}^{(6,2)} = -\left(y_2^2 + x_2^2\right)\left(x_1 y_2^3 + 3x_2 y_1 y_2^2 - 3x_1 x_2^2 y_2 - x_2^3 y_1\right), \tag{A5bb}$$

$$z_{ee}^{(6,3)} = -4x_2\left(y_1^2 + x_1^2\right) y_2 (y_2 - x_2)(y_2 + x_2), \tag{A5cc}$$

$$z_{ee}^{(6,4)} = -2(x_1 y_2 + x_2 y_1)(y_1 y_2 - x_1 x_2)\left(y_2^2 + x_2^2\right), \tag{A5dd}$$

$$z_{ee}^{(6,5)} = -\left(y_1^2 + x_1^2\right)\left(x_1 y_2^3 + 3x_2 y_1 y_2^2 - 3x_1 x_2^2 y_2 - x_2^3 y_1\right), \tag{A5ee}$$

$$z_{ee}^{(6,6)} = -\left(3x_1 y_1^2 y_2 - x_1^3 y_2 + x_2 y_1^3 - 3x_1^2 x_2 y_1\right)\left(y_2^2 + x_2^2\right), \tag{A5ff}$$

$$z_{ee}^{(6,7)} = -2\left(y_1^2 + x_1^2\right)(x_1 y_2 + x_2 y_1)(y_1 y_2 - x_1 x_2), \tag{A5gg}$$

$$z_{ee}^{(6,8)} = -4x_1 y_1 (y_1 - x_1)(y_1 + x_1)\left(y_2^2 + x_2^2\right), \tag{A5hh}$$

$$z_{ee}^{(6,9)} = -\left(y_1^2 + x_1^2\right)\left(3x_1 y_1^2 y_2 - x_1^3 y_2 + x_2 y_1^3 - 3x_1^2 x_2 y_1\right), \tag{A5ii}$$

$$\begin{aligned} z_{ee}^{(6,10)} = {} & -\left(5x_1 y_1^4 y_2 - 10x_1^3 y_1^2 y_2 + x_1^5 y_2 - x_2 y_1^5\right. \\ & \left. + 10x_1^2 x_2 y_1^3 - 5x_1^4 x_2 y_1\right), \end{aligned} \tag{A5jj}$$

$$z_{ee}^{(6,11)} = (x_1 y_2 + x_2 y_1)\left(y_2^2 + x_2^2\right)^2, \tag{A5kk}$$

$$z_{ee}^{(6,12)} = -\left(y_2^2 + x_2^2\right)\left(x_1 y_2^3 - 3x_2 y_1 y_2^2 - 3x_1 x_2^2 y_2 + x_2^3 y_1\right), \tag{A5ll}$$

$$z_{ee}^{(6,13)} = 2x_1 y_1\left(y_2^2 + x_2^2\right)^2, \tag{A5mm}$$

$$z_{ee}^{(6,14)} = 2x_2\left(y_1^2 + x_1^2\right) y_2\left(y_2^2 + x_2^2\right), \tag{A5nn}$$

$$z_{ee}^{(6,15)} = -2\left(x_1 y_2^2 - 2x_2 y_1 y_2 - x_1 x_2^2\right)\left(y_1 y_2^2 + 2x_1 x_2 y_2 - x_2^2 y_1\right), \tag{A5oo}$$

$$z_{ee}^{(6,16)} = \left(3x_1 y_1^2 y_2 - x_1^3 y_2 - x_2 y_1^3 + 3x_1^2 x_2 y_1\right)\left(y_2^2 + x_2^2\right), \tag{A5pp}$$

$$z_{ee}^{(6,17)} = \left(y_1^2 + x_1^2\right)(x_1 y_2 + x_2 y_1)\left(y_2^2 + x_2^2\right), \tag{A5qq}$$

$$z_{ee}^{(6,18)} = -\left(y_1^2 + x_1^2\right)\left(x_1 y_2^3 - 3x_2 y_1 y_2^2 - 3x_1 x_2^2 y_2 + x_2^3 y_1\right), \tag{A5rr}$$

$$z_{ee}^{(6,19)} = 2\left(2x_1 y_1 y_2 - x_2 y_1^2 + x_1^2 x_2\right)\left(y_1^2 y_2 - x_1^2 y_2 + 2x_1 x_2 y_1\right), \tag{A5ss}$$

$$z_{ee}^{(6,20)} = 2x_1 y_1\left(y_1^2 + x_1^2\right)\left(y_2^2 + x_2^2\right), \tag{A5tt}$$

$$z_{ee}^{(6,21)} = 2x_2\left(y_1^2 + x_1^2\right)^2 y_2, \tag{A5uu}$$

$$z_{ee}^{(6,22)} = \left(y_1^2 + x_1^2\right)\left(3x_1 y_1^2 y_2 - x_1^3 y_2 - x_2 y_1^3 + 3x_1^2 x_2 y_1\right), \tag{A5vv}$$

$$z_{ee}^{(6,23)} = \left(y_1^2 + x_1^2\right)^2 (x_1 y_2 + x_2 y_1). \tag{A5ww}$$

These symmetrized polynomials are used to express the three types of functions $\mathcal{F} \in \{\mathcal{V}, \mathcal{W}, \mathcal{Z}\}$, each expressed as

$$\begin{aligned} \mathcal{F} = {} & \mathcal{F}_a + \mathcal{F}_b + \mathcal{F}_{ee} + \mathcal{F}_{aee} + \mathcal{F}_{bee} + \mathcal{F}_{abee} \\ & + \sum_{i=1}^{2} \mathcal{F}_{e_i} + \mathcal{F}_{ae_i} + \mathcal{F}_{be_i} + \mathcal{F}_{abe_i}. \end{aligned} \tag{A6}$$

Here, a symbolizes the totally symmetric a_1' stretching coordinate and b is the a_2'' symmetric umbrella angle. Polynomials of a are invariant in any order, while the symmetry requires that only even powers of b are allowed. Therefore, using the expansion terms given above and in previous works,[50,51] the many-body terms up to 6th order can be written as

$$\mathcal{F}_a = \sum_{j=1}^{6} p_{f,a}^{(j)}\, a^j, \tag{A7a}$$

$$\mathcal{F}_b = \sum_{j=1}^{3} p_{f,b}^{(j)}\, b^{2j}, \tag{A7b}$$

$$\mathcal{F}_{e_i} = \sum_{j=1}^{6} \sum_{k} p_{f,e_i}^{(j,k)}\, f_{e_i}^{(j,k)}, \tag{A7c}$$

$$\mathcal{F}_{ee} = \sum_{j=1}^{6} \sum_{k} p_{f,ee}^{(j,k)}\, f_{ee}^{(j,k)}, \tag{A7d}$$

$$\vdots$$

$$\mathcal{F}_{aee} = \sum_{i=2}^{6} \sum_{j=1}^{i-1} \sum_{k} p_{f,aee}^{(i,j,k)}\, a^j\, f_{ee}^{(i-j,k)}, \tag{A7e}$$

$$\mathcal{F}_{bee} = \sum_{i=3}^{6} \sum_{j=1}^{(i-1)/2} \sum_{k} p_{f,bee}^{(i,j,k)}\, b^{2j}\, f_{ee}^{(i-2j,k)} \tag{A7f}$$

$$\vdots$$

in which $f \in \{v, w, z\}$. The expansion coefficients $p_{f,\ldots}^{(\ldots)}$ are the free parameters determined by fitting as discussed in Sec. II D. Note that $p_{w,\ldots}^{(\ldots)} = p_{z,\ldots}^{(\ldots)}$ due to the symmetry requirements.

[1] *Conical Intersections: Electronic Structure, Dynamics and Spectroscopy*, edited by W. Domcke, D. R. Yarkony, and H. Köppel (World Scientific, Singapore, 2004).
[2] H. C. Longuet-Higgins, *Advance in Spectroscopy* (Interscience, New York, 1961), Vol. 2, P. 429.
[3] W. Lichten, Phys. Rev. **131**, 229 (1963).
[4] W. Lichten, Phys. Rev. **164**, 131 (1967).
[5] F. T. Smith, Chem. Rev. **179**, 111 (1969).
[6] M. Baer, Chem. Phys. **15**, 49 (1976).
[7] H. Werner and W. Meyer, J. Chem. Phys. **74**, 5802 (1981).
[8] C. A. Mead and D. G. Truhlar, J. Chem. Phys. **77**, 6090 (1982).
[9] C. A. Mead, J. Chem. Phys. **78**, 807 (1983).

[10]H.-J. Werner, B. Follmeg, and M. H. Alexander, J. Chem. Phys. **89**, 3139 (1988).
[11]T. Pacher, L. S. Cederbaum, and H. Köppel, J. Chem. Phys. **89**, 7367 (1988).
[12]T. Pacher, C. A. Mead, L. S. Cederbaum, and H. Köppel, J. Chem. Phys. **91**, 7057 (1989).
[13]T. Pacher, H. Köppel, and L. S. Cederbaum, J. Chem. Phys. **95**, 6668 (1991).
[14]T. Pacher, L. S. Cederbaum, and H. Köppel, Adv. Chem. Phys. **84**, 293 (1993).
[15]H. Köppel, W. Domcke, and L. S. Cederbaum, Adv. Chem. Phys. **57**, 59 (1984).
[16]M. Baer, Chem. Phys. Lett. **35**, 112 (1975).
[17]W. Eisfeld and K. Morokuma, J. Chem. Phys. **113**, 5587 (2000).
[18]E. Wigner and J. Griffin, *Group Theory and Its Application to the Quantum Mechanics of Atomic Spectra*, Pure and Applied Physics (Academic Press, 1959).
[19]A. Thiel and H. Köppel, J. Chem. Phys. **110**, 9371 (1999).
[20]A. J. C. Varandas, F. B. Brown, C. A. Mead, D. G. Truhlar, and N. C. Blais, J. Chem. Phys. **86**, 6258 (1987).
[21]G. Hirsch, R. J. Buenker, and C. Petrongolo, Mol. Phys. **70**, 835 (1990).
[22]R. Cimiraglia, J. P. Malrieu, M. Persico, and F. Spiegelmann, J. Phys. B: At., Mol. Opt. **18**, 3073 (1985).
[23]W. Domcke and C. Woywod, Chem. Phys. Lett. **216**, 362 (1993).
[24]G. J. Atchity and K. Ruedenberg, Theo. Chem. Acc. **97**, 47 (1997).
[25]R. G. Sadygov and D. R. Yarkony, J. Chem. Phys. **109**, 20 (1998).
[26]H. Nakamura and D. G. Truhlar, J. Chem. Phys. **115**, 10353 (2001).
[27]H. Nakamura and D. G. Truhlar, J. Chem. Phys. **117**, 5576 (2002).
[28]R. Abrol and A. Kuppermann, J. Chem. Phys. **116**, 1035 (2002).
[29]H. Nakamura and D. G. Truhlar, J. Chem. Phys. **118**, 6816 (2003).
[30]M. S. Schuurman and D. R. Yarkony, J. Chem. Phys. **127**, 094104 (2007).
[31]B. N. Papas, M. S. Schuurman, and D. R. Yarkony, J. Chem. Phys. **129**, 124104 (2008).
[32]X. Zhu and D. R. Yarkony, J. Chem. Phys. **130**, 234108 (2009).
[33]X. Zhu and D. R. Yarkony, J. Chem. Phys. **132**, 104101 (2010).
[34]X. Zhu and D. R. Yarkony, J. Chem. Phys. **136**, 174110 (2012).
[35]H. Lischka, M. Dallos, P. G. Szalay, D. R. Yarkony, and R. Shepard, J. Chem. Phys. **120**, 7322 (2004).
[36]M. Barbatti, G. Granucci, M. Persico, and H. Lischka, Chem. Phys. Lett. **401**, 276 (2005).
[37]M. Barbatti, G. Granucci, M. Persico, M. Ruckenbauer, M. Vazdar, M. Eckert-Maksic, and H. Lischka, J. Photoch. Photobio. A **190**, 228 (2007).
[38]M. A. Collins and D. F. Parsons, J. Chem. Phys. **99**, 6756 (1993).
[39]J. Ischtwan and M. A. Collins, J. Chem. Phys. **100**, 8080 (1994).
[40]C. R. Evenhuis and M. A. Collins, J. Chem. Phys. **121**, 2515 (2004).
[41]C. R. Evenhuis, X. Lin, D. H. Zhang, D. Yarkony, and M. A. Collins, J. Chem. Phys. **123**, 134110 (2005).
[42]O. Godsi, C. R. Evenhuis, and M. A. Collins, J. Chem. Phys. **125**, 104105 (2006).
[43]B. J. Braams and J. M. Bowman, Int. Rev. Phys. Chem. **28**, 577 (2009).
[44]X. Zhu, J. Y. Ma, D. R. Yarkony, and H. Guo, J. Chem. Phys. **136**, 234301 (2012).
[45]J. Ma, X. Zhu, H. Guo, and D. R. Yarkony, J. Chem. Phys. **137**, 22A541 (2012).
[46]C. Xie, J. Ma, X. Zhu, D. H. Zhang, D. R. Yarkony, D. Xie, and H. Guo, J. Phys. Chem. Lett. **5**, 1055 (2014).
[47]J. Li, B. Jiang, and H. Guo, J. Chem. Phys. **139**, 204103 (2013).
[48]B. Jiang and H. Guo, J. Chem. Phys. **139**, 054112 (2013).
[49]V. C. Mota and A. J. C. Varandas, J. Phys. Chem. A **112**, 3768 (2008).
[50]A. Viel and W. Eisfeld, J. Chem. Phys. **120**, 4603 (2004).
[51]W. Eisfeld and A. Viel, J. Chem. Phys. **122**, 204317 (2005).
[52]A. Viel, W. Eisfeld, S. Neumann, W. Domcke, and U. Manthe, J. Chem. Phys. **124**, 214306 (2006).
[53]A. Viel, W. Eisfeld, C. R. Evenhuis, and U. Manthe, Chem. Phys. **347**, 331 (2008).
[54]A. V. Marenich and J. E. Boggs, J. Chem. Phys. **122**, 024308 (2005).
[55]A. V. Marenich and J. E. Boggs, Chem. Phys. Lett. **404**, 351 (2005).
[56]D. Opalka and W. Domcke, Chem. Phys. Lett. **494**, 134 (2010).
[57]D. Opalka and W. Domcke, J. Chem. Phys. **132**, 154108 (2010).
[58]R. P. Wayne, I. Barnes, P. Biggs, J. P. Burrows, C. E. Canosamas, J. Hjorth, G. Lebras, G. K. Moortgat, D. Perner, G. Poulet, G. Restelli, and H. Sidebottom, Atmos. Environ., Part A **25**, 1 (1991).
[59]W. Eisfeld and K. Morokuma, J. Chem. Phys. **114**, 9430 (2001).
[60]W. Eisfeld and K. Morokuma, J. Chem. Phys. **119**, 4682 (2003).
[61]M. Mayer, L. S. Cederbaum, and H. Köppel, J. Chem. Phys. **100**, 899 (1994).
[62]J. F. Stanton, J. Chem. Phys. **126**, 134309 (2007).
[63]S. Mahapatra, W. Eisfeld, and H. Köppel, Chem. Phys. Lett. **441**, 7 (2007).
[64]S. Faraji, H. Köppel, W. Eisfeld, and S. Mahapatra, Chem. Phys. **347**, 110 (2008).
[65]J. F. Stanton, Mol. Phys. **107**, 1059 (2009).
[66]J. F. Stanton and M. Okumura, Phys. Chem. Chem. Phys. **11**, 4742 (2009).
[67]A. D. Walsh, J. Chem. Soc. **1953**, 2301.
[68]A. Weaver, D. W. Arnold, S. E. Bradforth, and D. M. Neumark, J. Chem. Phys. **94**, 1740 (1991).
[69]A. Deev, J. Sommar, and M. Okumura, J. Chem. Phys. **122**, 224305 (2005).
[70]K. Takematsu, N. C. Eddingsaas, D. J. Robichaud, and M. Okumura, Chem. Phys. Lett. **555**, 57 (2013).
[71]P. J. Knowles, C. Hampel, and H.-J. Werner, J. Chem. Phys. **99**, 5219 (1993).
[72]T. H. Dunning, Jr., J. Chem. Phys. **90**, 1007 (1989).
[73]R. A. Kendall, T. H. Dunning, Jr., and R. J. Harrison, J. Chem. Phys. **96**, 6796 (1992).
[74]K. Kaufmann, W. Baumeister, and M. Jungen, J. Phys. B **22**, 2223 (1989).
[75]H.-J. Werner and W. Meyer, J. Chem. Phys. **73**, 2342 (1980).
[76]H.-J. Werner and W. Meyer, J. Chem. Phys. **74**, 5794 (1981).
[77]P. J. Knowles and H.-J. Werner, Chem. Phys. Lett. **145**, 514 (1988).
[78]H.-J. Werner and P. J. Knowles, J. Chem. Phys. **89**, 5803 (1988).
[79]H.-J. Werner, P. J. Knowles, R. Lindh, F. R. Manby, M. Schütz *et al.*, MOLPRO, version 2009.1, a package of *ab initio* programs, 2009, see http://www.molpro.net.
[80]E. R. Davidson, J. Comput. Phys. **17**, 87 (1975).
[81]D. Whitley, Stat. Comput. **4**, 65 (1994).
[82]W. H. Press, S. A. Teukolsky, and W. T. Vetterling, *Numerical Recipes in FORTRAN 77* (Cambridge University Press, Cambridge, 1992).
[83]H. D. Meyer, U. Manthe, and L. S. Cederbaum, Chem. Phys. Lett. **165**, 73 (1990).
[84]U. Manthe, H. D. Meyer, and L. S. Cederbaum, J. Chem. Phys. **97**, 3199 (1992).
[85]G. Schiffel and U. Manthe, J. Chem. Phys. **132**, 084103 (2010).
[86]R. Wodraszka, J. Palma, and U. Manthe, J. Phys. Chem. A **116**, 11249 (2012).
[87]U. Manthe, J. Chem. Phys. **105**, 6989 (1996).
[88]U. Manthe, J. Chem. Phys. **128**, 064108 (2008).
[89]D. Forney, W. E. Thompson, and M. E. Jacox, J. Chem. Phys. **99**, 7393 (1993).